

Washington University School of Medicine

**Digital Commons@Becker**

---

Open Access Publications

---

2021

**Pyrazole scaffold synthesis, functionalization, and applications in Alzheimer's disease and Parkinson's disease treatment (2011-2020)**

Xuefei Li

Yanbo Yu

Zhude Tu

Follow this and additional works at: [https://digitalcommons.wustl.edu/open\\_access\\_pubs](https://digitalcommons.wustl.edu/open_access_pubs)

---

Review

# Pyrazole Scaffold Synthesis, Functionalization, and Applications in Alzheimer's Disease and Parkinson's Disease Treatment (2011–2020)

Xuefei Li, Yanbo Yu  and Zhude Tu \*

Department of Radiology, Washington University School of Medicine,  
510 S. Kingshighway Boulevard St. Louis, MO, 63110, USA; xuefeili@wustl.edu (X.L.);  
yanboyu@wustl.edu (Y.Y.)

\* Correspondence: zhudetu@wustl.edu; Tel.: +1-314-362-8487

**Abstract:** The remarkable prevalence of pyrazole scaffolds in a versatile array of bioactive molecules ranging from apixaban, an anticoagulant used to treat and prevent blood clots and stroke, to bixafen, a pyrazole-carboxamide fungicide used to control diseases of rapeseed and cereal plants, has encouraged both medicinal and organic chemists to explore new methods in developing pyrazole-containing compounds for different applications. Although numerous synthetic strategies have been developed in the last 10 years, there has not been a comprehensive overview of synthesis and the implication of recent advances for treating neurodegenerative disease. This review first presents the advances in pyrazole scaffold synthesis and their functionalization that have been published during the last decade (2011–2020). We then narrow the focus to the application of these strategies in the development of therapeutics for neurodegenerative diseases, particularly for Alzheimer's disease (AD) and Parkinson's disease (PD).

**Keywords:** pyrazole; synthesis; functionalization; heterocyclic; neurodegeneration; Alzheimer's disease; Parkinson's disease; inhibitor; antagonist; biological activity



**Citation:** Li, X.; Yu, Y.; Tu, Z. Pyrazole Scaffold Synthesis, Functionalization, and Applications in Alzheimer's Disease and Parkinson's Disease Treatment (2011–2020). *Molecules* **2021**, *26*, 1202. <https://doi.org/10.3390/molecules26051202>

Academic Editors: Vera L. M. Silva, Artur M. S. Silva and Cosimo Damiano Altomare

Received: 11 January 2021  
Accepted: 22 February 2021  
Published: 24 February 2021

**Publisher's Note:** MDPI stays neutral with regard to jurisdictional claims in published maps and institutional affiliations.



**Copyright:** © 2021 by the authors. Licensee MDPI, Basel, Switzerland. This article is an open access article distributed under the terms and conditions of the Creative Commons Attribution (CC BY) license (<https://creativecommons.org/licenses/by/4.0/>).

## 1. Introduction

Pyrazole compounds contain a five-membered aromatic ring composed of three carbon atoms and two adjacent nitrogen atoms. The shifting C-N double bond inside the heterocycle endows pyrazoles with tautomerism. Consequently, regioselectivity can be a challenge in the synthesis and purification of *N*-substituted and asymmetric pyrazoles. Although a pyrazole core is rare in natural compounds, artificial pyrazole derivatives are prevalent in diverse fields. Applications range from agrochemicals [1] to therapeutics. At least thirty-three pyrazole-containing medicines have been marketed to alleviate or treat diseases ranging from bacterial infections to cancer and neurologic disorder (Figure 1) [2,3]. For example, the anticoagulant apixaban is used to prevent serious blood clots that may cause stroke, heart attack, and is also prescribed to patients with an abnormal heartbeat (atrial fibrillation) or hip/knee joint replacement surgery; in 2018, apixaban was the second most popular blockbuster drug [4]. Investigators in both academic institutions and pharmaceutical industries have put tremendous efforts into the exploration of new pyrazole scaffolds for drug development. This review, building upon previous literature, reviews [3,5] and presents progress in the chemical synthesis of pyrazole scaffold molecules and the functionalization of pyrazole derivatives from 2011 to 2020. We then focus on pyrazole-containing small biomolecules developed as therapeutic candidates for treating neurodegenerative diseases, particularly those that target pathologies found in Alzheimer's disease (AD) and Parkinson's disease (PD). Fluorine-18 radiotracers composed of pyrazole scaffolds have been recently reviewed by Gomes and his colleagues [6] and will not be discussed in this review.

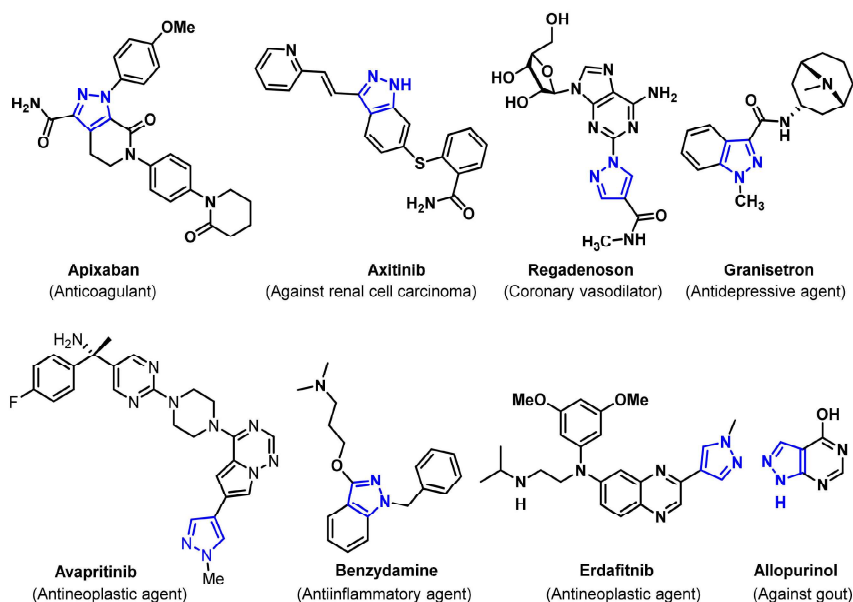
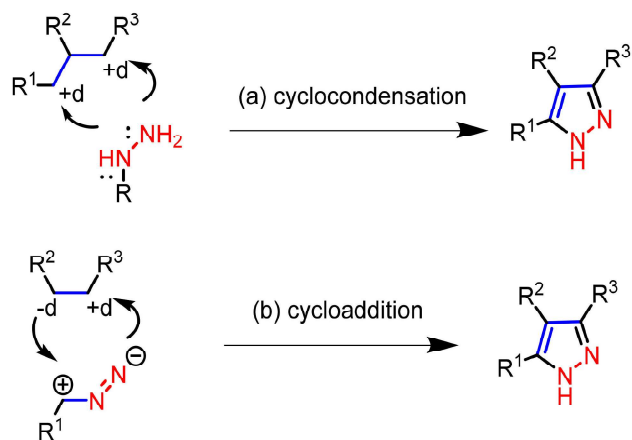


**Figure 1.** Representative FDA-approved pyrazole-containing medicines. FDA: U.S. Food and Drug Administration.

## 2. The Synthesis of Pyrazole Scaffold Molecules

The synthesis of substituted pyrazoles has been accomplished by two strategies [3,5]: (1) the cyclocondensation of hydrazines with 1,3-dicarbonyl compounds or their synthetic 1,3-dielectrophilic equivalents (Scheme 1a), and (2) the cycloaddition of 1,3-dipoles to dipolarophiles (Scheme 1b). These two conventional strategies were recently enriched by additional approaches including multicomponent one-pot processes, photoredox reactions, and transition-metal catalyzed reactions. In this section, we will first discuss cyclocondensation, followed with cycloaddition. In addition, new approaches are also discussed.



**Scheme 1.** Conventional pyrazole synthetic strategies. (a): cyclocondensation; (b): cycloaddition.

### 2.1. Cyclocondensation of Hydrazines with 1,3-Dielectrophilic Derivatives

Substituted or nonsubstituted hydrazines are readily available as [NN] synthons for the synthesis of pyrazole derivatives. Pyrazole molecules can be generated through hydrazines reacting with 1,3-dielectrophilic units such as 1,3-dicarbonyl or with  $\alpha,\beta$ -unsaturated carbonyl compounds; the latter structures include enones, ynones, and vinyl ketones bearing a leaving group (Figure 2) [3].

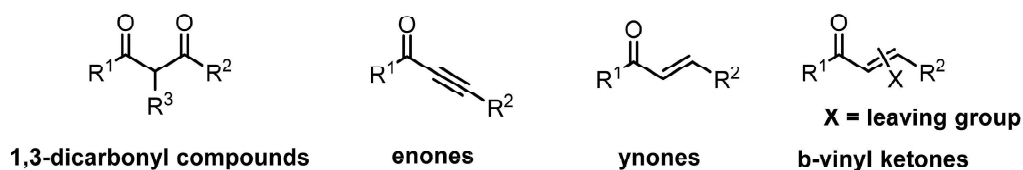
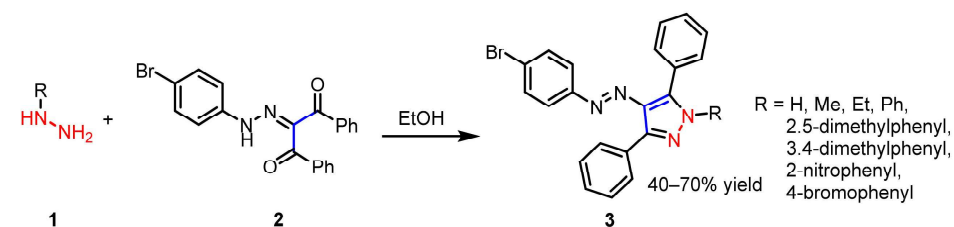


**Figure 2.** Structures of 1,3-dielectrophilic derivatives.

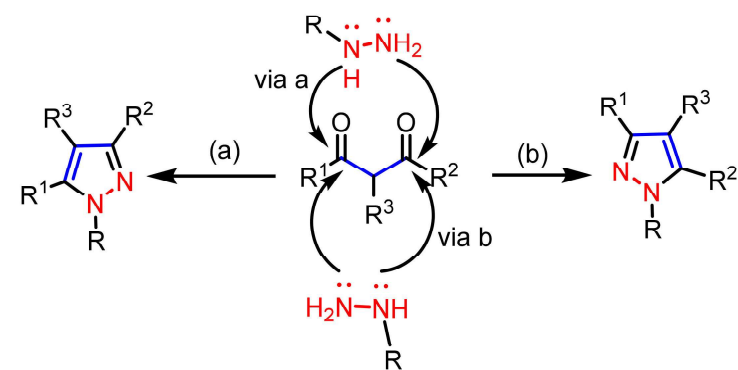
### 2.1.1. Cyclocondensation of Hydrazines with 1,3-Dicarbonyl and Related Compounds

1,3-diketones,  $\beta$ -ketoesters, 2,4-diketoesters, and related synthetic equivalents can condense efficiently with hydrazines to generate substituted pyrazoles. Based on this strategy, a series of potent carbonic anhydrase,  $\alpha$ -glycosidase, and cholinesterase enzymes inhibitors **1** were synthesized via the cyclocondensation of the 1,3-diketone and appropriate hydrazines (Scheme 2) [7].



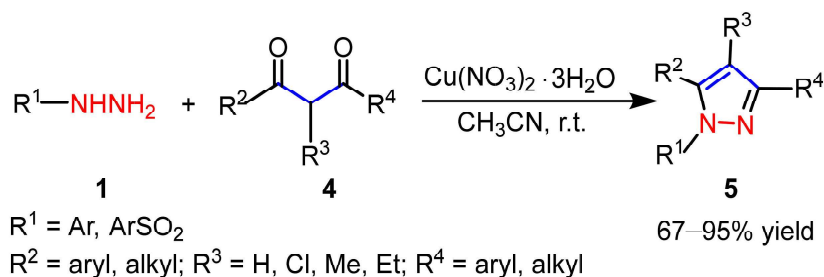
**Scheme 2.** Bioactive molecules synthesis by cyclocondensation.

However, a mixture of two regioisomers is produced in most cases when unsymmetrical 1,3-dicarbonyl compounds ( $R^1 \neq R^2$ ), and substituted hydrazines are used for cyclocondensation (Scheme 3). Moreover, this kind of cyclocondensation is generally accomplished in a strongly acidic medium (i.e., fluoroboric acid [8]), thus the reaction solution is corrosive and not environmentally-friendly.



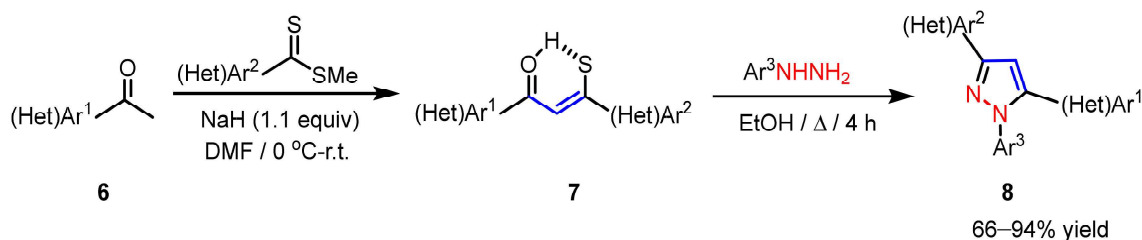
**Scheme 3.** Regioselectivity of pyrazoles synthesis via cyclocondensation.

A mild and acid-free condensation of 1,3-diketones with substituted hydrazines to generate the 1,3,5-trisubstituted and fully substituted pyrazoles was reported by Wang and co-workers [9]. The optimal conditions were obtained when using copper (II) nitrate as the catalyst, providing the cyclocondensation products at room temperature in less than 60 min. More importantly, this method provided highly regioselective products with good yields (Scheme 4).



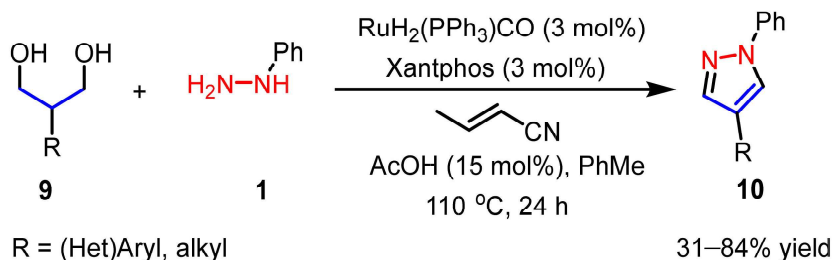
**Scheme 4.** Cu-catalyzed cyclocondensation for pyrazole synthesis.

As a novel derivative of 1,3-dicarbonyl compounds, 1,3-monothiodiketones are good complements for preparing unsymmetrically substituted 1-aryl-3,5-bis(het)arylpyrazoles with excellent regioselectivity and high yield (Scheme 5) [10].



**Scheme 5.** 1,3-monothiodiketones as substrates for pyrazole synthesis.

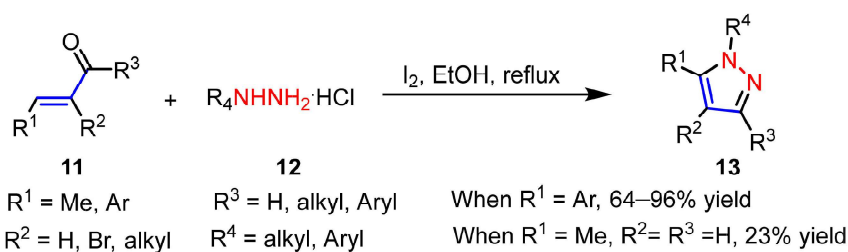
Despite the efficiency and flexibility of using 1,3-dicarbonyl compounds as substrates, the synthetic inconvenience and inherent instability of many 1,3-dicarbonyls, particularly dialdehydes, limits the synthesis of some substituted pyrazoles. To overcome this challenge, Schmitt et al. reported the facile generation of 1,4-disubstituted pyrazoles when using ruthenium as a catalyst with 1,3-diols to replace 1,3-dicarbonyl compounds [11]. In this reaction, crotonitrile was used as the reductant to accept hydrogen transfer from ruthenium dihydrides (Scheme 6).



**Scheme 6.** 1,3-diols as substrates for pyrazole synthesis.

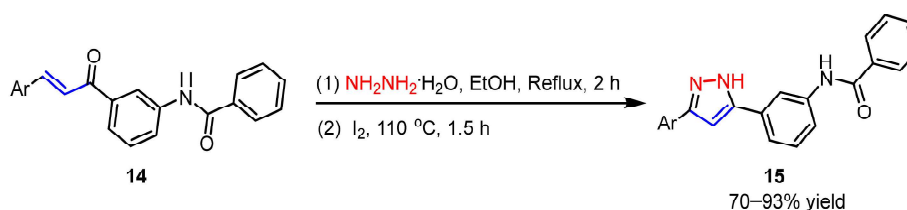
### 2.1.2. Cyclocondensation of Hydrazines with Enones and Related Compounds

The condensation of hydrazines with  $\alpha$ -enones affords pyrazolines, and can be followed by oxidation to generate the corresponding pyrazoles. Zhang et al. reported using iodine to mediate oxidative intramolecular C-N bond formation, and the hydrazone intermediates were cyclized to generate pyrazoles [12]. This one-pot applicable procedure led directly to a variety of di-, tri-, and tetra-substituted (aryl, alkyl, and/or vinyl) pyrazole derivatives with high (64–96%) yields when using  $\beta$ -aryl substituted aldehydes and ketones as substrates. However, the yield decreased sharply when  $\text{R}^1$  was a methyl group (23% yield) due to the loss of the extended conjugation to facilitate the nucleophilic attack of the  $\alpha,\beta$ -unsaturated double-bond to iodine (Scheme 7).



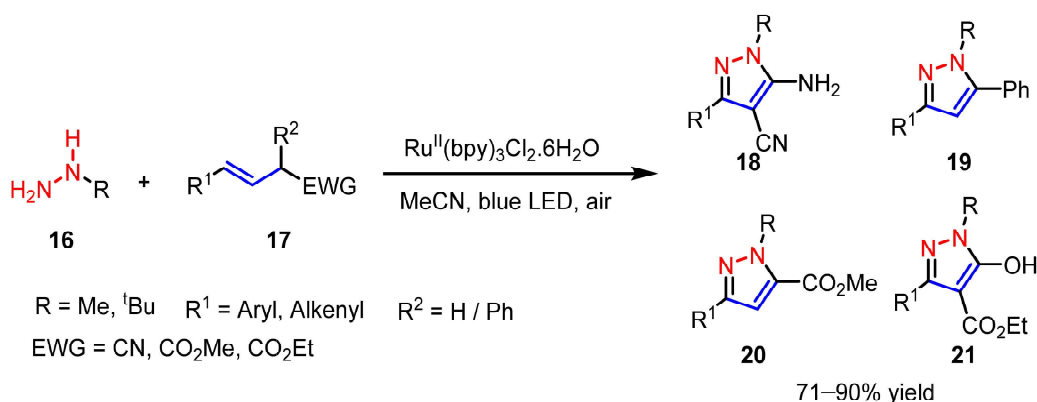
**Scheme 7.** I<sub>2</sub>-mediated cyclocondensation for pyrazole synthesis.

The applicability of this general method has been extended to synthesize an array of novel 3,5-diarylpyrazole derivatives (**15**); some of these are potent acetylcholinesterase inhibitors possessing excellent selectivity, and have been accepted as prospective drug candidates for treating Alzheimer's disease (Scheme 8) [13].



**Scheme 8.** 3,5-diarylpyrazole synthesis through I<sub>2</sub>-mediated cyclocondensation.

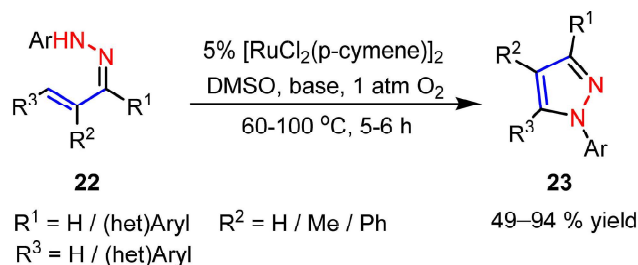
In addition, Ding et al. reported an air-promoted photoredox cyclization of substituted hydrazines with activated alkene (Michael addition reaction acceptors) to afford corresponding pyrazoles with good to excellent yields [14]. In this context, hydrazine was oxidized by Ru<sup>II</sup> to a diazene intermediate that attacks Michael acceptors, followed by an intramolecular cyclization to form pyrazoles. The reduced Ru<sup>I</sup> was reoxidized by air to recycle this photoredox process. For electron withdrawing groups (EWG) such as cyano or carboxylic acid groups, this procedure efficiently generated 5-amino and 5-hydroxyl substituted pyrazoles, which are important functionalities for subsequent transformations (Scheme 9).



**Scheme 9.** Ru<sup>II</sup>-catalyzed photoredox cyclization for pyrazole synthesis.

Pre-installation of enones with hydrazines to form hydrazone intermediates is also accessible. Hu and co-workers [15] reported a Ru<sup>II</sup>-catalyzed intramolecular oxidative C–N coupling for the facile synthesis of highly diversified tri- and tetrasubstituted pyrazoles. Their method is applicable to a broad scope of substrates with excellent functional group

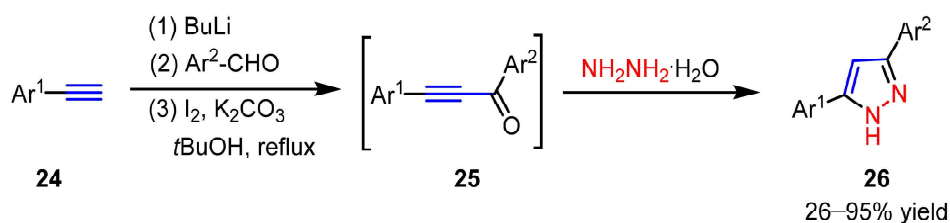
tolerance. More importantly, many of the pyrazoles generated using this strategy were difficult to prepare by conventional methods (Scheme 10).



**Scheme 10.**  $\text{Ru}^{\text{II}}$ -catalyzed oxidative cyclization for pyrazoles synthesis.

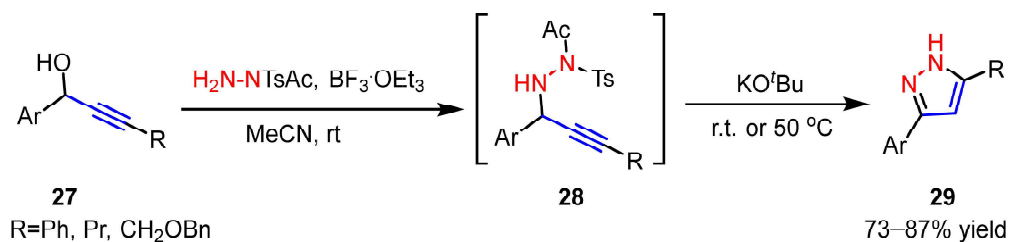
### 2.1.3. Cyclocondensation of Hydrazines with Ynones and Related Compounds

Harigae et al. reported using a one-pot regioselective procedure for the synthesis of 3,5-disubstituted pyrazoles with good yields [16]. In his multicomponent procedure, ynone intermediates were formed through iodine-mediated in situ oxidation of propargylic alcohols that were converted from terminal alkynes and aldehydes (Scheme 11).



**Scheme 11.** Multicomponent synthesis of pyrazoles from alkynes.

In addition, propargylic alcohols, the reduced form of ynones, were also used to generate 3,5-disubstituted 1*H*-pyrazoles [17]. This procedure includes two consecutive steps: (1) Lewis acid catalyzed *N*-propargylation of propargylic alcohols to propargyl hydrazides with *N*-acetyl-*N*-tosylhydrazine, followed by (2) base-mediated intramolecular cyclization (Scheme 12).



**Scheme 12.** Propargylic alcohols as substrates for two-step pyrazole synthesis.

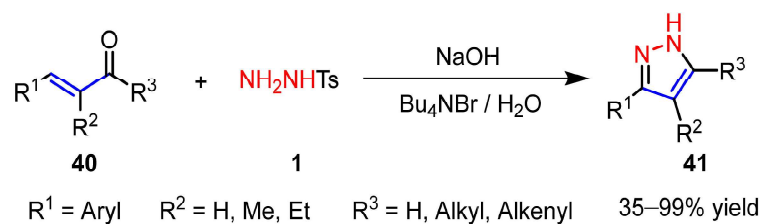
### 2.1.4. Cyclocondensation of Hydrazines with Vinyl Ketones Bearing a Leaving Group

Aminomethylene and (dimethyl)aminomethylene groups are synthetic equivalents of a formyl group.  $\alpha, \beta$ -Vinyl ketones containing these substituents may react with hydrazine derivatives to afford pyrazolines, followed by elimination of the leaving group to generate the desired pyrazoles. The methylthio group has also been reported as an excellent leaving group [10]. Guo et al. reported that in the presence of iodine and *tert*-butyl hydroperoxide (TBHP),  $\beta$ -amino vinyl ketone could cyclize with tosyl hydrazine in water to afford fully substituted pyrazoles [18]. Mechanism studies using  $^{15}\text{N}$ -labeled enaminone as a substrate





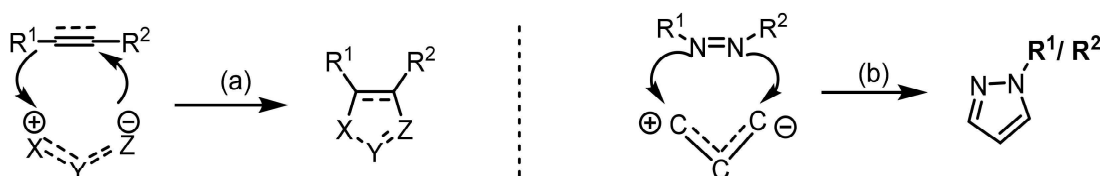
the phase transfer catalyst  $\text{Bu}_4\text{NBr}$  is used, these reactions can be performed smoothly in water [22] (Scheme 16).



**Scheme 16.** Proton leaving groups in cyclocondensation for pyrazole synthesis.

### 2.2. 1,3-Dipolar Cycloadditions

The intrinsically high regioselectivity and efficiency of 1,3-dipolar cycloaddition has led to its prominent role in preparing substituted pyrazoles [5]. Conventional 1,3-dipolar cycloaddition employs a [CNN] fragment and a [CC] fragment. In general, three main classes of 1,3-dipoles have been used as the [CNN] fragment, namely, diazoalkanes, nitrilimines, and azomethine imines, while their [CC] counterparts are alkenes or alkynes (Scheme 17a). Additionally, the combination of a [CCC] fragment plus a [NN] fragment has also been utilized. In these examples, [CCC] comes from alkenes or alkynes, while the [NN] fragment derives from azo compounds (Scheme 17b).

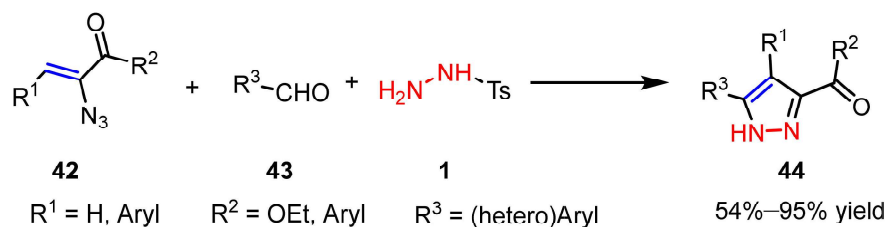


**Scheme 17.** Strategies for 1,3-dipolar cycloaddition. (a): [CNN] + [CC] mode; (b): [CCC] + [NN] mode.

In this section, we discuss the synthetic development of 1,3-dipolar cycloaddition reactions according to the source of 1,3-dipoles fragments, namely, from diazoalkanes, nitrilimines, or azomethine imine, respectively. Reactions in which azo compounds act as [NN] fragments are also presented.

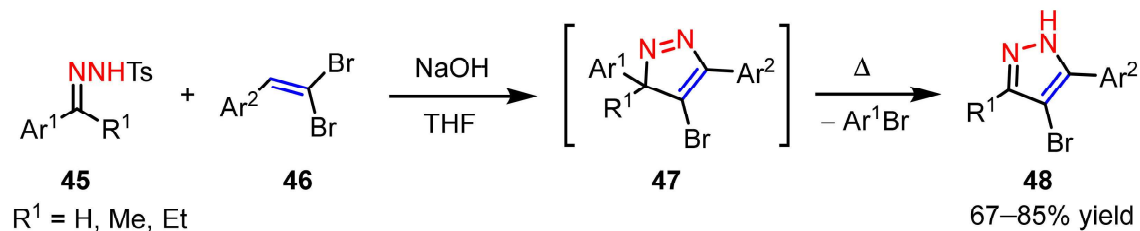
#### 2.2.1. Diazoalkanes as 1,3-Dipoles

Electron-rich diazo compounds are toxic and potentially explosive, thus the preparation and handling of these reactants are hazardous. To overcome this problem, an improved method for making aryldiazomethanes from stable tosylhydrazones derivatives was developed to synthesize pyrazoles. Using an operationally simple, multicomponent, one-pot procedure, 3,4,5-trisubstituted 1*H*-pyrazoles could be prepared from vinyl azide, aldehyde, and tosylhydrazine [23]. In these cases, the azide group serves as a leaving group (Scheme 18).



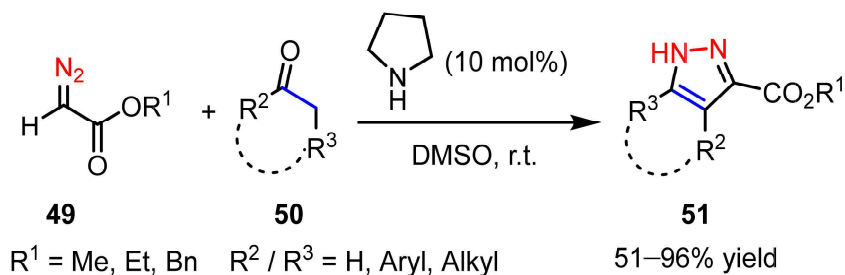
**Scheme 18.** Azide as leaving groups in diazoalkanes for pyrazole synthesis.

Bromine is also a good leaving group. Sha et al. developed a simple, highly efficient, and regioselective method for the synthesis of 3,5-diaryl-4-bromopyrazoles using *gem*-dibromoalkene as the substrate [24] (Scheme 19).



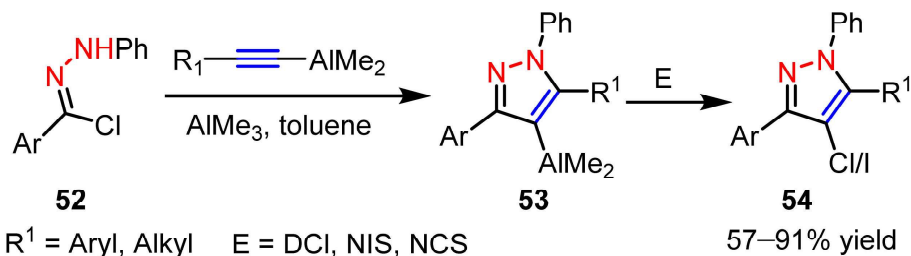
**Scheme 19.** Bromine as the leaving group in diazoalkanes for pyrazole synthesis.

Using pyrrolidine as a catalyst, 3,4,5-trisubstituted or 3,5-disubstituted pyrazoles could be synthesized from carbonyl compounds through an enamine intermediate under mild conditions [25]. Considering that carbonyl compounds are more readily available than alkenes, this optimization is a remarkable advancement. In addition, bicyclic pyrazoles that are difficult to synthesize by common methods can be prepared straightforwardly using this method (Scheme 20).



**Scheme 20.** Ketones as substrates in 1,3-dipolar cycloaddition for pyrazole synthesis.

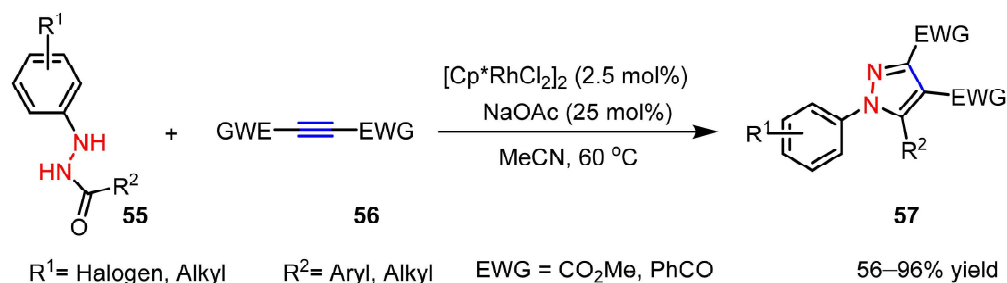
Jackowski et al. reported a novel method to synthesize organoaluminum heterocyclics via a [3 + 2] cycloaddition route [26]. Using this methodology, 3,4,5-trisubstituted pyrazoles could be prepared from reactive polysubstituted alumino-heteroles intermediates (53) after a one-step electrophilic substitution (Scheme 21).



**Scheme 21.** Trimethylaluminum substituted alkynes as substrates for pyrazoles synthesis.

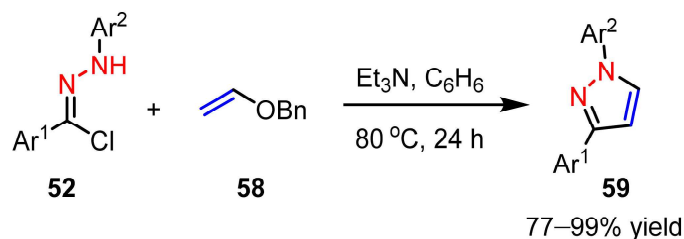
### 2.2.2. Nitrilimines as 1,3-Dipoles

Li and co-workers [27] reported a rhodium-catalyzed cycloaddition of hydrazines with dicarboxylic alkynes. This method provides a highly efficient and effective procedure to synthesize 3,4-dicarboxylic pyrazoles, and offering versatility for subsequent structural modifications (Scheme 22).



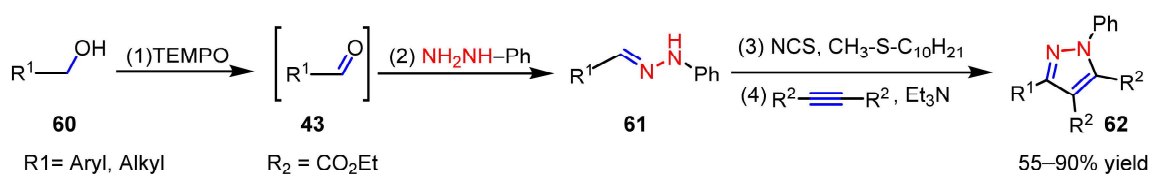
**Scheme 22.** Ru<sup>II</sup>-catalyzed 1,3-dipolar cycloaddition for pyrazole synthesis.

Ledovskaya et al. reported that the weak organic base trimethylamine (TEA) could promote the 1,3-dipolar cycloaddition of vinyl ethers and hydrazonoyl chlorides to produce 1,3-disubstituted pyrazoles with absolute regioselectivity [28] (Scheme 23).



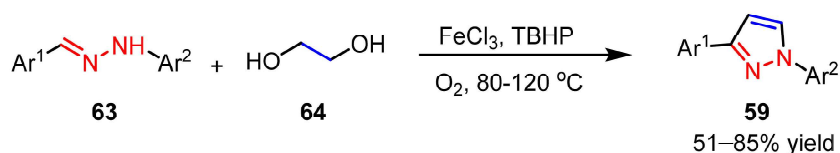
**Scheme 23.** Trimethylamine (TEA) promoted 1,3-dipolar cycloaddition for pyrazoles synthesis.

Starting from primary alcohols, Kobayashi et al. reported a one-pot, multicomponent procedure for making multisubstituted pyrazoles [29]. According to their description, the primary alcohol was first oxidized by 2,2,6,6-tetramethylpiperidinyloxy (TEMPO) to aldehyde, followed by reacting with hydrazine to form oxime, where the latter was converted into nitrilimine in the presence of *N*-chlorosuccinimide (NCS) and decyl methyl sulfide, followed by a 1,3-dipolar cycloaddition between nitrilimine and diethyl acetylenedicarboxylate (Scheme 24).



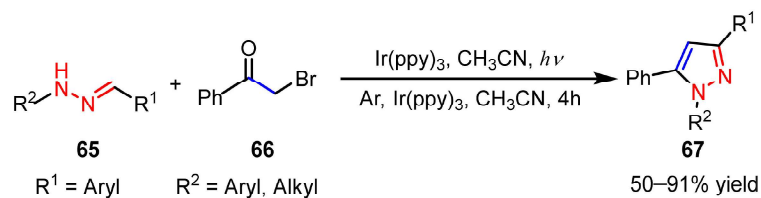
**Scheme 24.** Primary alcohols as substrates for pyrazole synthesis.

Using alcohols as potential [CC] fragments, Panda et al. reported an iron-catalyzed route [30] for the regioselective synthesis of 1,3- and 1,3,5-substituted pyrazoles by the condensation of diarylhydrazones with  $\alpha$ -carbonyl alcohols, which were converted in situ from vicinal diols by ferric chloride in the presence of *tert*-butyl hydroperoxide (TBHP) (Scheme 25).



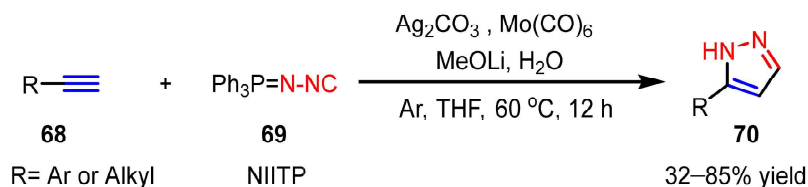
**Scheme 25.** Fe<sup>III</sup>-catalyzed 1,3-dipolar cycloaddition for pyrazole synthesis.

A one-pot visible light-promoted single-electron-transfer (SET) process for making 1,3,5-trisubstituted pyrazoles from  $\alpha$ -bromoketones was reported by Fan and co-workers [31]. The reaction has good functional group tolerance, even for nitro and nitrile, which are generally not tolerated in SET reactions (Scheme 26).



**Scheme 26.** Ir<sup>III</sup>-catalyzed photoredox cycloaddition for pyrazole synthesis.

Yi et al. reported a novel silver-mediated [3 + 2] cycloaddition of alkynes and *N*-isocyanoiminotriphenylphosphorane (NIITP) for the assembly of monosubstituted pyrazoles [32]. The reaction can be accomplished under mild conditions, with broad substrate scope and excellent functional group tolerance. Mechanism studies showed that NIITP was activated by Mo(CO)<sub>6</sub>, then undergoes a [3 + 2] cycloaddition with a silver acetylide intermediate (Scheme 27).



**Scheme 27.** Ag<sup>II</sup>-mediated cycloaddition for pyrazole synthesis.

Bioactive molecules with pyrrolopyrazole motifs such as an aurora kinase inhibitor danusertib (71), a glycine transporter-1 inhibitor (72), an HIV-1 integrase inhibitor (73), and an antibacterial agent (74) are promising drug candidates [33] (Figure 3). Therefore, general and practical methods for making such compounds are valuable.

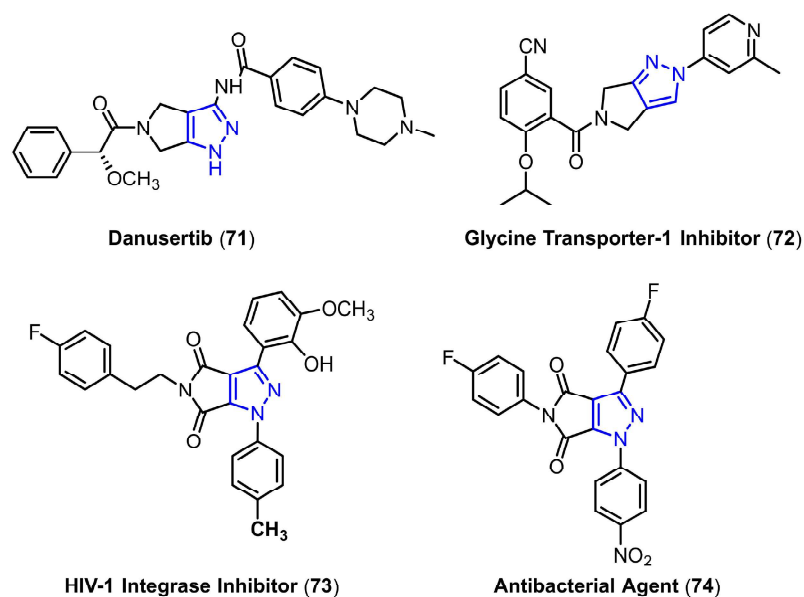
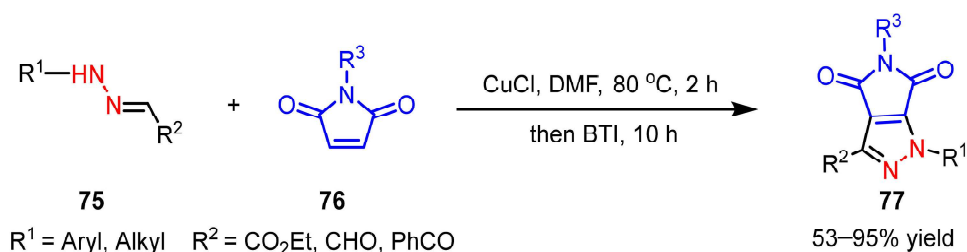


**Figure 3.** Bioactive molecules containing pyrrolopyrazole motifs.

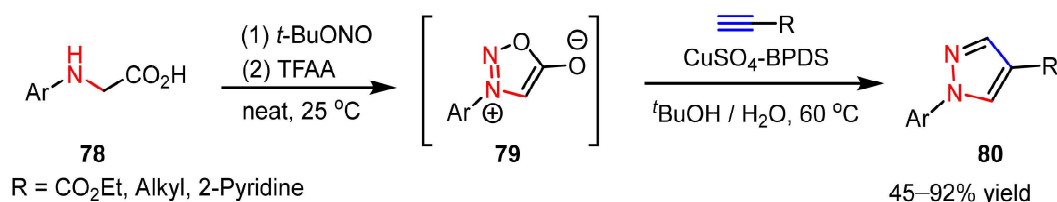
Zhu et al. reported a CuCl-catalyzed oxidative coupling reaction of aldehyde hydrazones with maleimides to prepare dihydropyrazoles under mild conditions [33]. Using this method, a variety of pyrrolo[3,4-*c*]pyrazoles could be obtained from dihydropyrazoles by one-step following oxidation (Scheme 28).



**Scheme 28.** Cu<sup>I</sup>-catalyzed cycloaddition for pyrrolopyrazole synthesis.

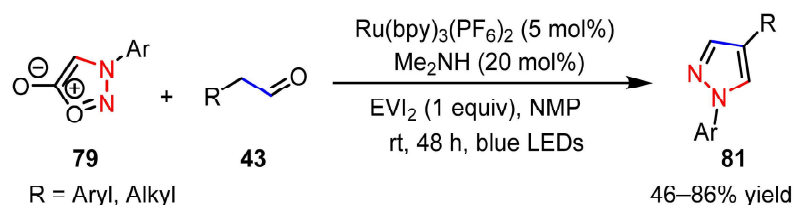
### 2.2.3. Sydnone as 1,3-Dipoles

Specklin et al. reported a one-pot Cu-catalyzed sydnone-alkyne cycloaddition to generate 1,4-disubstituted pyrazoles from readily available arylglycines [34]. This method tolerates various electron-rich or electron-poor *N*-aryl sydnones, and acetylene components. Using this method, 1,4-pyrazoles were the only products with good to excellent yield; no trace of 1, 3-regioisomers was detected (Scheme 29).



**Scheme 29.** Sydnone as 1,3-dipoles for pyrazole synthesis.

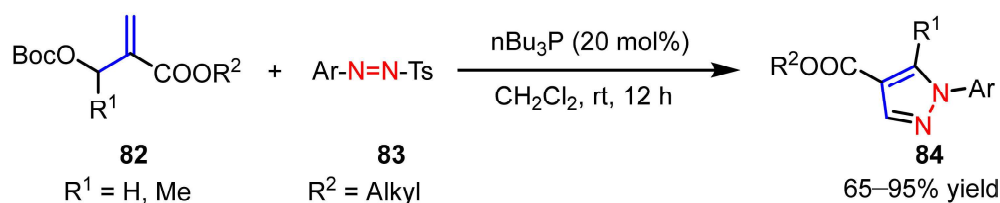
In addition, a visible-light photoredox process using Ru(bpy)<sub>3</sub>(PF<sub>6</sub>)<sub>2</sub> as the catalyst to accomplish this regioselective reaction was also reported. In this case, a broad scope of 1,4-disubstituted pyrazoles was made in high yields [35] (Scheme 30).



**Scheme 30.** Ru<sup>II</sup>-catalyzed photoredox cycloaddition for pyrazole synthesis.

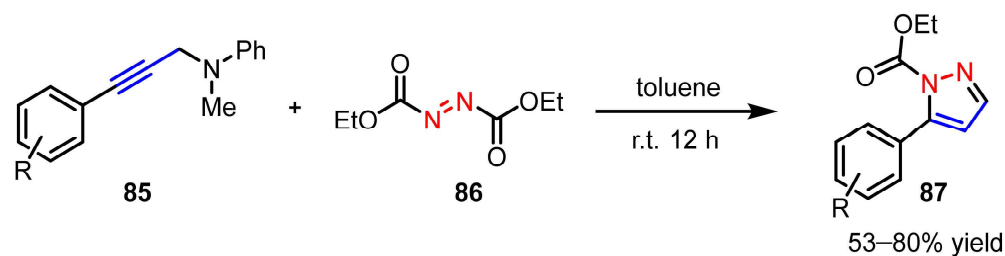
### 2.2.4. Azo Compounds as [NN] Fragments

Zhang et al. reported a highly efficient *n*Bu<sub>3</sub>P-catalyzed desulfonylative [3 + 2] cycloadditions of allylic carbonates with arylazosulfones to make 1,4-disubstituted pyrazoles in good to excellent yields under mild conditions [36]. The reaction can be triggered by the Michael-type addition of *n*Bu<sub>3</sub>P to allylic carbonate, meanwhile, an allylic phosphorus ylide intermediate was formed after decomposition of the Boc group into CO<sub>2</sub> and *t*BuOH. The ylide intermediate subsequently underwent a [3 + 2] cycloaddition with arylazosulfones to afford the substituted pyrazoles (Scheme 31).



**Scheme 31.** Azo compounds as [NN] fragment for pyrazole synthesis.

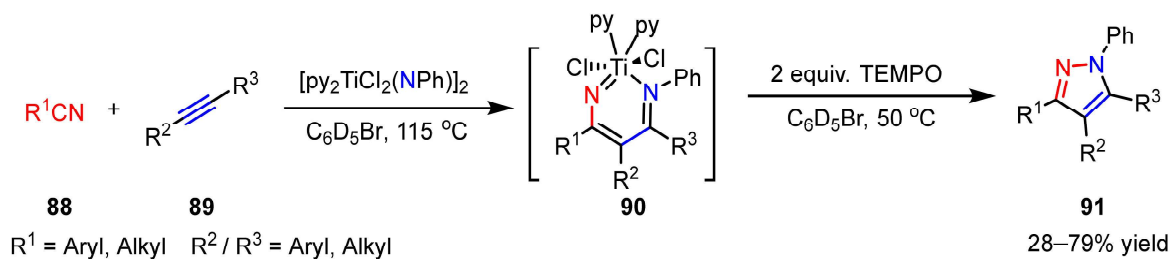
For some reactions, the involvement of organophosphorus in azo-type cycloadditions is useful, but not essential. Zhang and co-workers [37] reported that substituted propargylamines could react with commercially available dialkyl azodicarboxylates (DEAD) in toluene at room temperature without the presence of organophosphorus. This synthetic strategy was also applicable for the synthesis of different pyrazoles in high yields with broad substrate scopes (Scheme 32).



**Scheme 32.** Dialkyl azodicarboxylates (DEAD) as substrates in cycloaddition for pyrazole synthesis.

### 2.3. New Approaches to Reactions for Pyrazole Synthesis

In each of the above-mentioned methodologies for pyrazole synthesis, all the [NN] fragments either came from hydrazine derivatives or from azo compounds. Pearce and co-workers recently reported a novel fragment combination mode [NC] + [CC] + [N] using a multicomponent oxidative coupling to make multi-substituted pyrazoles [38]. In these reactions, diazatitana-cyclohexadiene intermediates that were generated from alkynes, nitriles, and titanium imido complexes, could produce pyrazole derivatives after a 2-electron oxidation process triggered by oxidant TEMPO (Scheme 33).



**Scheme 33.** Organotitanium intermediates for pyrazole synthesis.

## 3. The Functionalization of Pyrazoles

### 3.1. The Synthesis of Fluorine-Containing and Fluoroalkyl Substituted Pyrazoles

The incorporation of fluorine or fluoroalkyl groups onto a pyrazole ring [1,39] can positively affect its physicochemical and biological properties. Exploration of these compounds has led to the successful commercial application of numerous fluorine-containing pyrazoles, as shown in Figure 4. Therefore, new methods of synthesizing fluorine containing pyrazoles may facilitate new drug discoveries, both in pharmaceutical and agrochemical

industries. In addition, the incorporation of fluorine in pyrazole motifs can enable  $^{18}\text{F}$ -labeling for preclinical and clinical position emission tomography (PET) applications. As Gomes et al. have published a recent detailed review on this topic [6], we will not discuss it in this manuscript.

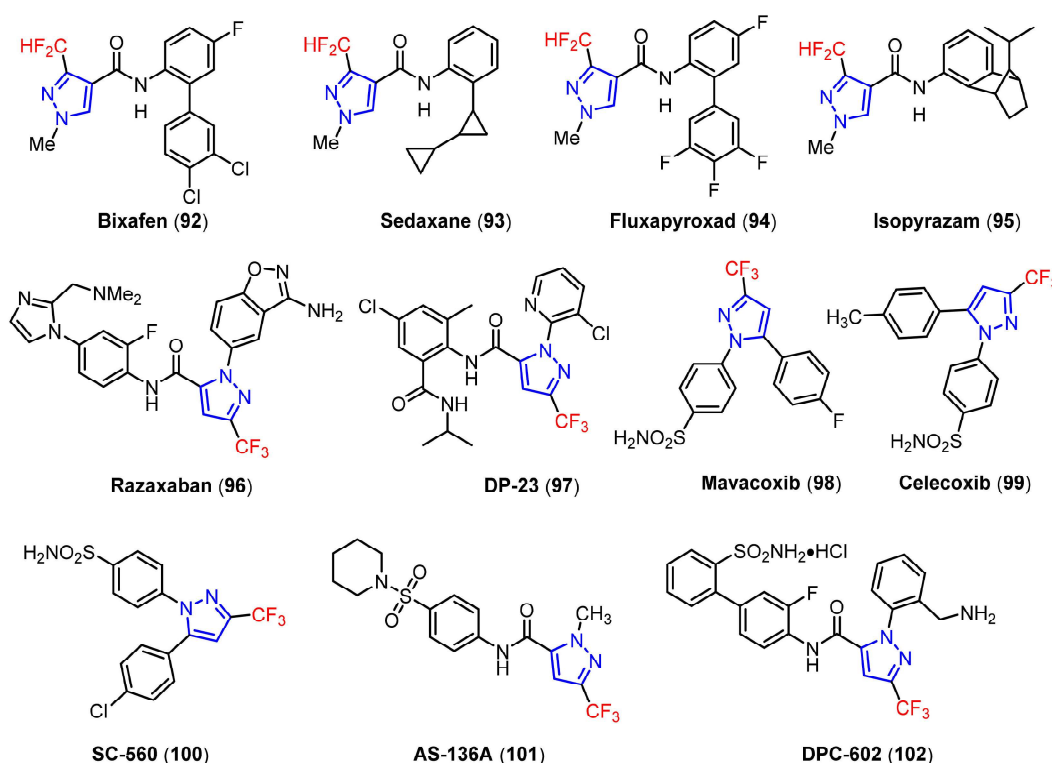
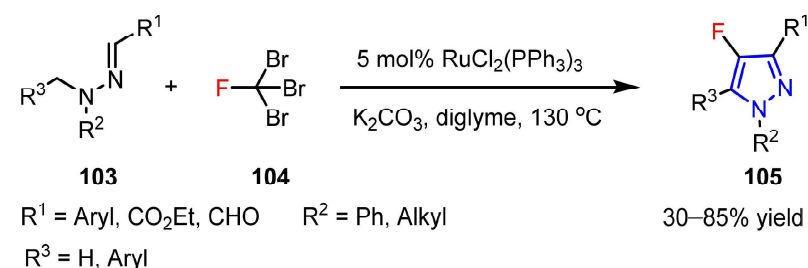


**Figure 4.** Examples of bioactive molecules with fluorine-containing pyrazole moieties.

### 3.1.1. The Synthesis of Monofluorine-Substituted Pyrazoles

Prieto and co-workers [40] described an accessible method to synthesize 4-fluoropyrazoles by ruthenium-catalyzed tandem C–H fluoromethylation and cyclization of *N*-alkylhydrazones. In this context,  $\text{CBr}_3\text{F}$  was acting as the fluorine source and a one-carbon unit. Compared to a range of other transition-metal catalysts (Cu, Pd, and Fe),  $\text{RuCl}_2(\text{PPh}_3)_3$  was the most efficient for this reaction (Scheme 34).



**Scheme 34.**  $\text{Ru}^{\text{II}}$ -catalyzed synthesis of monofluorine substituted pyrazoles.

### 3.1.2. The Synthesis of Difluoromethylpyrazoles

Difluoromethyl-substituted pyrazoles are valuable scaffolds for the preparation of fungicides in agriculture (Figure 4) [1]. Recently, industrial materials like ethyl 2,2-difluoroacetate and fluoroalkyl amino reagents (FAR) (Figure 5) have been widely employed as building blocks for making difluoromethyl pyrazoles [41,42].

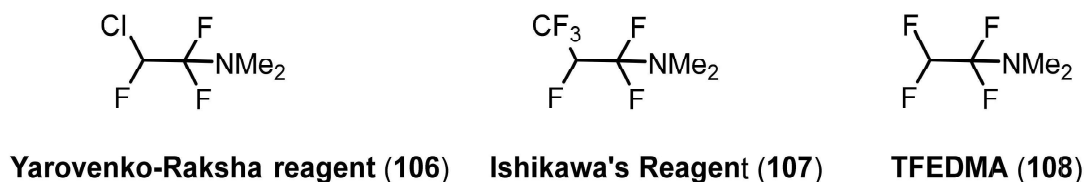
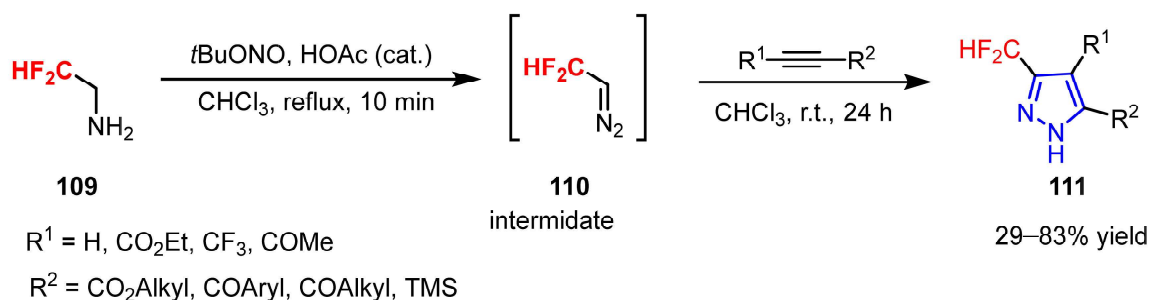


**Figure 5.** Representative fluoroalkyl amino reagents.

Mykhailiuk [43] reported a novel approach to preparing difluoromethyl-substituted pyrazoles by a [3 + 2] cycloaddition between alkynes and  $\text{CF}_2\text{HCHN}_2$ , which was generated in situ from readily available  $\text{CF}_3\text{CH}_2\text{NH}_2$ . This practical methodology uses a two-step, one-pot procedure, and does not require either the involvement of a catalyst, or the isolation of a potentially toxic and explosive gaseous intermediate. More importantly, this operationally feasible approach supports scale-up synthesis of target pyrazoles (Scheme 35).



**Scheme 35.** Synthesis of difluoromethyl pyrazoles.

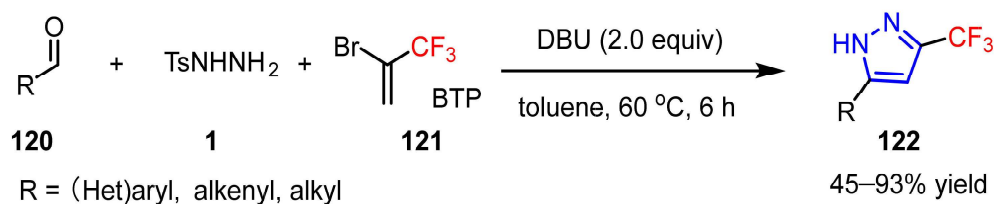
### 3.1.3. The Synthesis of Trifluoromethyl Pyrazoles

Among fluorinated pyrazoles, the synthesis of 3-trifluoromethyl pyrazoles has attracted significant attention because trifluoromethyl, a strong electronic withdraw group, may increase the bioactivity of target molecules. The feasibility of this tactic is evidenced by the success of a variety of pharmaceuticals and agrochemicals such as razaxaban (**96**, anti-coagulant), and DP-23 (**97**, insecticidal activity), mavacoxi (**98**) and celecoxib (**99**) (both are COX-2 inhibitors), and SC-560 (**100**, human lung cancer inhibitor), AS-136A (**101**, measles virus inhibitor), and DPC-602 (**102** arterial thrombosis) (Figure 4). Conventional synthetic methods often suffer from poor regioselectivity between the 3-isomer and 5-isomer when using trifluoromethyl substituted 1,3-dicarbonyl compounds as starting materials [44].

Li et al. reported a highly regioselective approach to the synthesis of 3-trifluoromethyl pyrazoles using silver-mediated cycloaddition of alkynes with 2,2,2-trifluorodiazethane, which is generated from readily available  $\text{CF}_3\text{CH}_2\text{NH}_2\cdot\text{HCl}$  [45]. This mild procedure is applicable for the synthesis of celecoxib and measles virus inhibitor AS-136. Interestingly, the reaction only proceeds well in the presence of a trace amount of water (0.1–1 equivalent), otherwise, the yield decreased sharply in the presence of either no water or too much water (>10 equivalent). A deuterated substitution experiment suggested that the proton on 4-position is abstracted from the water medium. Further mechanism studies indicated that silver acetylide might be the active species, as the addition of silver oxide was essential to facilitate this cycloaddition reaction (Scheme 36).

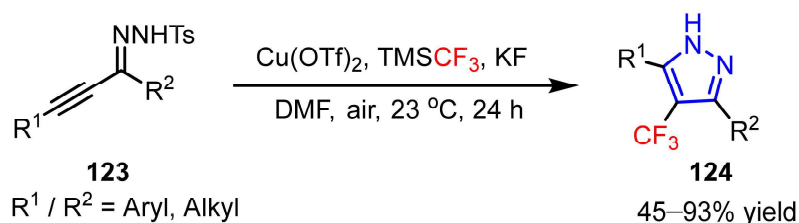






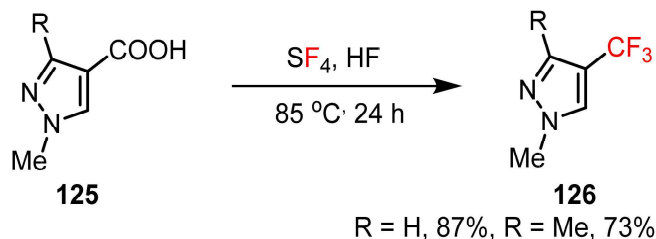
**Scheme 40.** 2-bromo-3,3,3-trifluoropropene (BTP) as a building block for the synthesis of 3-trifluoromethylpyrazoles.

Wang and co-workers [49] reported a mild method of synthesizing 4-(trifluoromethyl)pyrazoles in high yields; this copper-mediated method, using nucleophilic trifluoromethyltrimethylsilane (TMS $\text{CF}_3$ ) as the  $\text{CF}_3$  source, is an important supplement to electrophilic trifluoromethylation reactions (Scheme 41).



**Scheme 41.**  $\text{Cu}^{\text{II}}$ -mediated 4-trifluoromethylpyrazoles.

The above-mentioned methodologies offer great convenience in constructing trifluoromethylpyrazoles with various trifluoromethyl-containing building blocks and reagents. However, some of these trifluoromethyl-containing chemicals are expensive or potentially explosive [47,49]. Thus more straightforward methodologies like the direct fluorination of existing functional group into a trifluoromethyl have also been explored. For example, in the presence of HF, sulfur tetrafluoride can directly deoxofluoridize 4-pyrazolecarboxylic acids into corresponding 4-(trifluoromethyl)pyrazoles in high yields [50] (Scheme 42).



**Scheme 42.** Direct fluorination to synthesize 4-trifluoromethylpyrazoles.

### 3.2. N-Alkylation, N-Arylation, and N-Alkenylation of Pyrazoles

The direct *N*-alkylation of pyrazoles to yield  $\alpha$ -pyrazole ketone derivatives is of great importance because of their pharmacological potential in diverse bioactive molecules. Examples including retinoic acid receptor-related orphan receptor gamma ( $\text{ROR}\gamma$ ) modulator 1 (127), Janus kinase (JAK) inhibitors (128) and (129), and insecticides (130) are shown in Figure 6 [51]. High regioselectivity in such transformations is readily achieved under optimized reaction conditions. In addition, any minor impurity of regioisomer can be removed easily due to the differences in its physical properties (e.g., polarity, solubility difference) to the main product during purification.

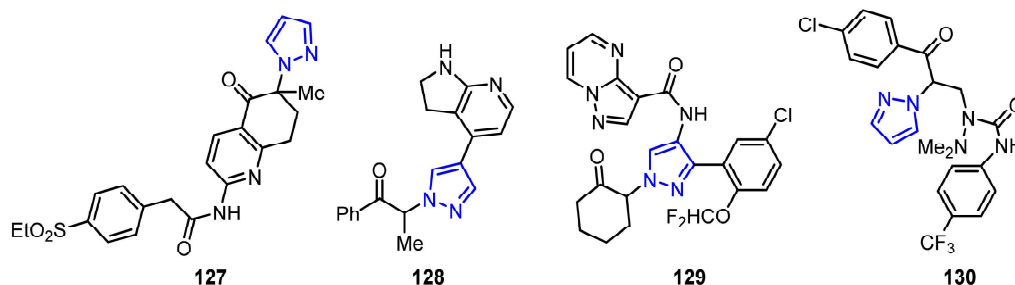
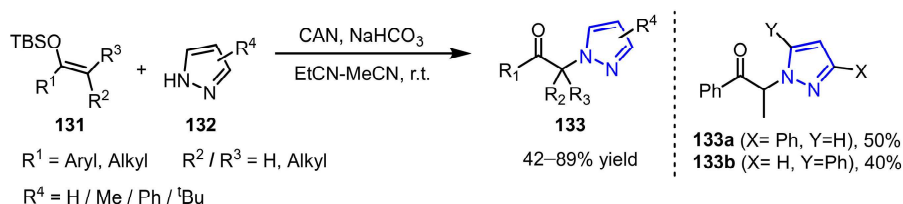


**Figure 6.** Applications of  $\alpha$ -pyrazole ketone scaffolds in bioactive molecules.

### 3.2.1. The Synthesis of *N*-Alkylated Pyrazoles

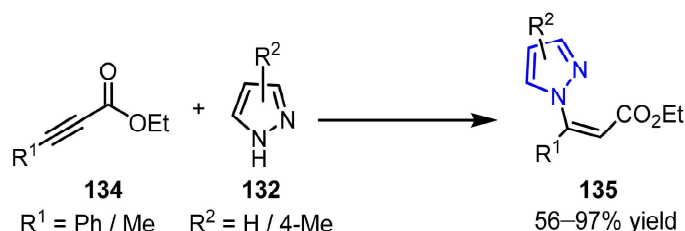
Dhanju et al. reported a general method of using ceric ammonium nitrate to mediate oxidative coupling of enolsilanes and heterocycles for making diverse  $\alpha$ -pyrazole ketones [51]. Interestingly, they found that under the same reaction conditions, quaternary  $\alpha$ -pyrazole ketone derivatives could be prepared; such pyrazole derivatives are not generally accessible via conventional synthetic methods due to steric hindrance (Scheme 43). Nevertheless, for some asymmetrical pyrazole substrates, this method generated a mixture of regioisomers. For example, **133a** and **133b** were synthesized in a ratio of 1.25:1. This is attributed to the conjugation effect of the phenyl group at the C<sub>2</sub> substitution of the pyrazole ring, the hyperconjugation inside the bicyclic ring system consisting of the pyrazole group, and the phenyl group accelerates the fast shifting of the C–N double bond between the two nitrogen atoms. The two flexible tautomeric structures tend to afford the product as a mixture of regioisomers in almost equal ratio. Conversely, other substitutions (i.e., H, *t*Bu) having no conjugation effect only provided a single regioisomer in high yield [51].



**Scheme 43.** *N*-alkylation of pyrazoles.

### 3.2.2. The Synthesis of *N*-Alkenylated Pyrazoles

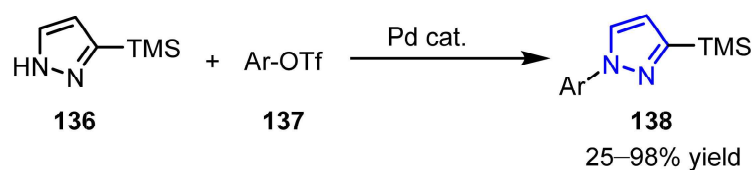
Compared to the *N*-alkylation and arylation of pyrazoles, few synthetic methods for *N*-alkenylation of pyrazoles were reported. In 2015, to prepare  $\beta$ -pyrazolyl acids possessing a wide range of bioactivities [52], Luo and co-workers [53] reported a gold-catalyzed stereoselective 1,4-conjugate addition of pyrazoles to propiolates to afford *N*-alkenyl substituted pyrazoles in moderate to good yields with high regioselectivity. Under optimized conditions, the undesired regioisomer ratio was <3% when using an unsubstituted pyrazole as the substrate. After hydrogenation of the double bond,  $\beta$ -pyrazolyl acid esters, the precursors of  $\beta$ -amino acids, could be obtained effortlessly (Scheme 44).



**Scheme 44.** *N*-alkenylation of pyrazoles.

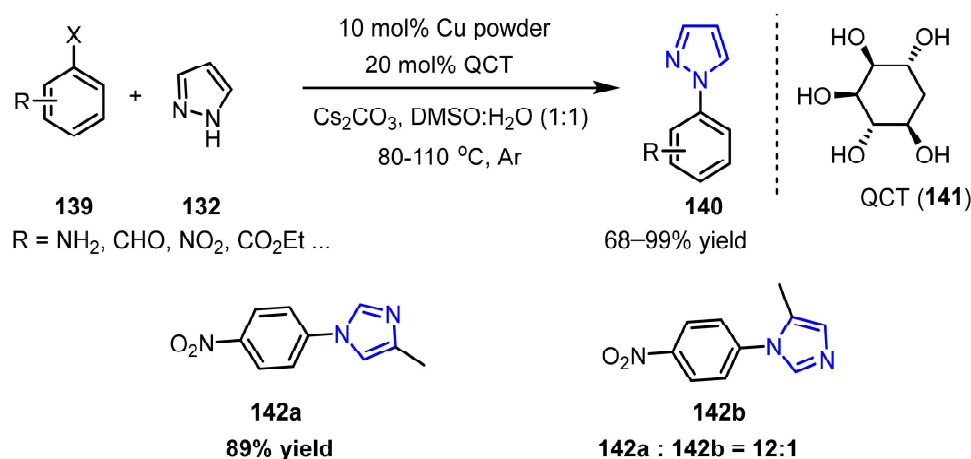
### 3.2.3. The Synthesis of *N*-Arylated Pyrazoles

*N*-arylpiperazines motifs are common in natural products, bioactive molecules, and pharmaceuticals [54]; furthermore, they are also prevalent components of auxiliary ligands for transition-metal catalysis [55]. Conventional methods of synthesizing *N*-arylpiperazines rely on using either Buchwald–Hartwig coupling [56] or classical Ullmann reactions [57], requiring noble palladium catalysts or harsh reaction conditions. Onodera et al. reported an efficient method using palladium-catalyzed coupling of aryl halides with 3-trimethylsilylpyrazole to make *N*-arylpiperazines in quantitative yields [58]. Interestingly, 3-trimethylsilyl substitution on pyrazole substrates is essential for high yields; in addition, 3-trimethylsilyl substitution also offers considerable synthetic potential and diversity for subsequent structural modifications (Scheme 45).



**Scheme 45.** Pd-catalyzed synthesis of *N*-arylated pyrazoles.

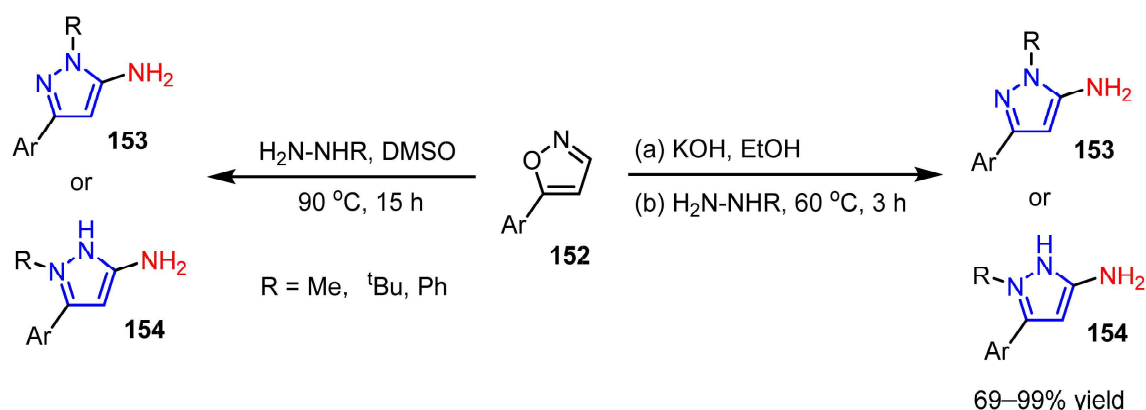
A general Cu-catalyzed Ullmann-type coupling to synthesize *N*-arylazoles was reported by Zhou and co-workers [59]; they discovered that using L-(-)-quebrachitol (QCT), a recycled waste in natural rubber industry as the *O, O*-bidentate ligand, both aryl bromides and aryl chlorides can afford *N*-arylpiperazines. In addition, aryl triflates that are readily made from phenolics were also well tolerated to prepare desired products in excellent yields (Scheme 46). Noticeably, using asymmetric imidazole having a tautomerism similar to pyrazole as the substrate, **142a** could be made in a high regioselective ratio of 12:1. This Cu powder involved catalytic system presented a superior regioselectivity and high yield compared to the Cu<sub>2</sub>O catalytic system [60]. Copper powder is more reactive in the Ullmann-type reaction than Cu<sub>2</sub>O as a catalyst. In addition, the ligand (QCT) can coordinate the in situ formed copper ions to stabilize the reaction intermediates, a more stable tautomeric structure. The collective roles have a net effect of a higher regioselectivity [59].



**Scheme 46.** Cu-catalyzed synthesis of *N*-arylated pyrazoles.

Wang et al. reported a metal-free oxidative methodology for the coupling of benzoxazoles and pyrazoles to form a bis-heterocyclic system of *N*<sub>1</sub>-benzoxazole substituted pyrazole derivatives [61]; the formation of radical species in the presence of oxidants is the common feature of such protocols (Scheme 47).

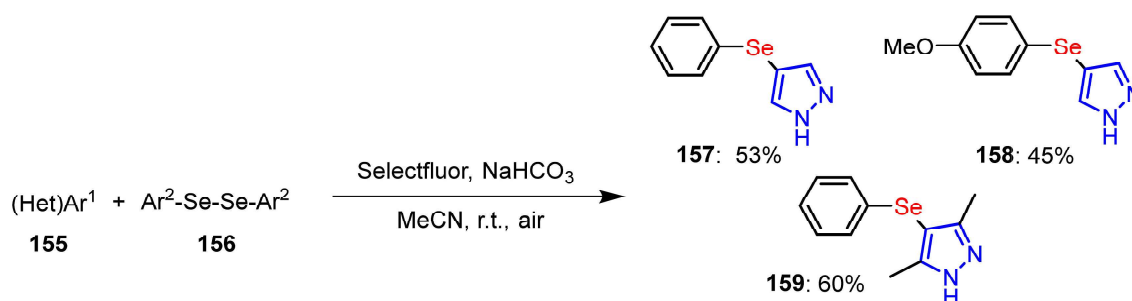




**Scheme 49.** Isoxazoles as substrates for 3-aminopyrazoles synthesis.

### 3.4. The Selanylation of Pyrazoles.

Emerging data from pharmacological studies and clinical trials reveal that seleno-proteins and organoselenium molecules are participating in a variety of physiological activities [65,66]. For example, a selenium-containing celecoxib derivative was shown to be effective in downregulating the transcription of COX-2 and other pro-inflammatory genes [67]. This highlighted the significance of incorporating selenium into pyrazole motifs. Belladonna et al. reported a direct C-H selanylation of pyrazoles with Selectfluor (*N*-chloromethyl-*N*-fluorotriethylenediammonium bis(tetrafluoroborate)), a stable and commercially available oxidant, to afford 4-phenylselenol substituted pyrazole derivatives [68]. The reaction was triggered by the interaction of diphenyl selenide with Selectfluor to form electrophilic selanyl species, which were then attacked by nucleophilic pyrazole substrates to give the final product. Mechanism studies suggest that the formation of a Se–F bond between Selectfluor and diselenide is the critical step to restrain the formation of non-fluorinated byproducts (Scheme 50).



**Scheme 50.** The synthesis of selanylated pyrazoles.

### 3.5. The Borylation of Pyrazoles

Borylated pyrazoles are critical building blocks in scalable Suzuki-coupling reactions for preparing pyrazole-containing pharmaceuticals and fine chemicals. Nevertheless, such starting chemicals are commercially scarce due to the unavailability of relevant synthetic methodologies. Recently, Wang and co-workers [69] described that dianthphos, an easily prepared monophosphine ligand, is capable of facilitating the Miyaura borylation of pyrazole substrates with high yields, but only two representatives were presented in their publication (Scheme 51).



#### 4.1.1. Acetylcholinesterase (AChE) Inhibitors

Acetylcholine (ACh) is a critical neurotransmitter and neuromodulator in the central nervous system (CNS), its relatively low concentration in the cerebral cortex of AD brains results in the degeneration of cholinergic neurons as well as the deficit of cholinergic neurotransmission [75]. In neurons, ACh is synthesized from choline and acetyl-CoA when catalyzed by choline acetyltransferase (ChAT) and is hydrolyzed into acetate and choline by acetylcholinesterase (AChE) [76]. AChE is primarily found at the synaptic cleft and the neuromuscular junction of the brain. In contrast, outside of the CNS, the cholinergic enzyme subtype butyrylcholinesterase (BuChE) mainly exists in blood plasma. Unlike the substrate specific AChE, BuChE can nonspecifically hydrolyze many different choline or non-choline based esters and amides [77]. The colocalization of AChE or BuChE with A $\beta$  aggregates in SPs could accelerate A $\beta$  aggregation, thus increasing neurotoxicity [78–80]. Therefore, cholinesterase inhibitors have been viewed as a promising target for AD treatment.

In 2018, Turkan et al. reported a series of substituted pyrazol-4-yl-diazene derivatives (**3**), and their *in vitro* enzymatic assay suggested that all were effective AChE and BuChE inhibitors with  $K_i$  values at the nanomole level, better than tacrine (**164**), a discontinued acetylcholinesterase inhibitor that was used to treat AD [7]. However, their poor selectivity between AChE and BuChE, and broad activities over  $\alpha$ -glycosidase and cytosolic carbonic anhydrase might be problematic. Shaikh et al. reported novel scaffolds of *N*-substituted pyrazole-derived  $\alpha$ -aminophosphonates, two of these compounds (**165**, **166**) exhibited strong potency against AChE and high selectivity over BuChE, and their performances were better than the commercially available drugs galantamine (**167**) and rivastigmine (**168**) [81]. Compound **169** had ~100-fold selectivity for AChE over BuChE, furthermore, it exhibited 45% neuroprotection ratio in rotenone/oligomycin A-induced neuronal death. When compared to tacrine, only a minor activity decrease was observed [82]. Gutti et al. reported a linear pyrazole derivative (**170**) as an AChE inhibitor in 2019 [13]. When tested in MC65 cells at 50  $\mu$ M, compound **170** improved cell viability by 90% and could reduce A $\beta_{1-42}$  aggregation induced by metals effectively at 20  $\mu$ M (Figure 8, Table 1).

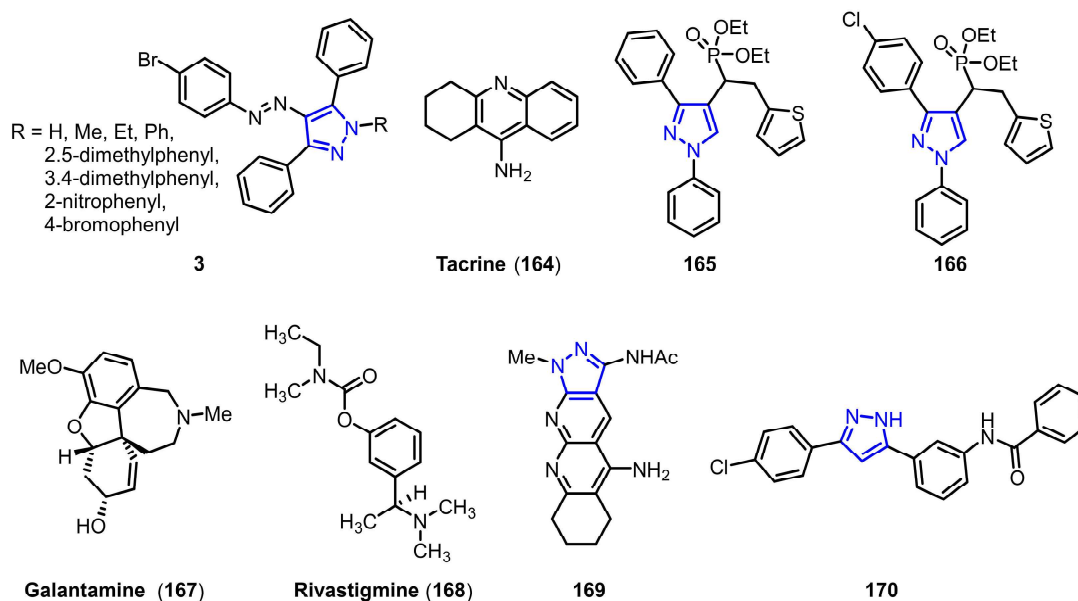


Figure 8. Chemical structures of cholinesterase inhibitors.



Table 1. Affinities of cholinesterase inhibitors.

$K_i^1$ or $IC_{50}^2$ Values for Cholinesterase Inhibitors				
Compound	R	AChE	BuChE	AChE/BuChE
<b>3a</b> <sup>1</sup>	H	58.17 ± 4.84 nM	74.82 ± 18.62 nM	0.77
<b>3b</b> <sup>1</sup>	Me	64.71 ± 13.04 nM	80.36 ± 22.74 nM	0.80
<b>3c</b> <sup>1</sup>	Et	47.93 ± 4.92 nM	58.12 ± 9.27 nM	0.82
<b>3d</b> <sup>1</sup>	Ph	44.66 ± 10.06 nM	50.36 ± 13.88 nM	0.88
<b>3e</b> <sup>1</sup>	2, 5-dimethylphenyl	78.34 ± 17.83 nM	77.62 ± 18.32 nM	1.00
<b>3f</b> <sup>1</sup>	3, 4-dimethylphenyl	48.16 ± 9.63 nM	65.27 ± 12.73 nM	0.73
<b>3g</b> <sup>1</sup>	2-nitrophenyl	56.23 ± 11.74 nM	71.63 ± 8.93 nM	0.78
<b>3h</b> <sup>1</sup>	4-bromophenyl	60.27 ± 15.67 nM	88.36 ± 20.03 nM	0.68
<b>164</b> <sup>1</sup>	–	126.13 ± 9.37 nM	145.84 ± 13.44 nM	0.86
<b>165</b> <sup>2</sup>	–	0.055 ± 0.143 μM	8.863 ± 0.22 μM	0.006
<b>166</b> <sup>2</sup>	–	0.017 ± 0.02 μM	6.331 ± 0.017 μM	0.003
<b>167</b> <sup>2</sup>	–	3.148 ± 0.139 μM	1.22 ± 0.05 μM	2.58
<b>168</b> <sup>2</sup>	–	2.632 ± 0.021 μM	6.901 ± 0.01 μM	0.38
<b>169</b> <sup>2</sup>	–	0.069 ± 0.06 μM	6.3 ± 0.6 μM	0.01
<b>170</b> <sup>2</sup>	–	1937 ± 66 nM	1166 ± 88 nM	1.60

<sup>1</sup> The values shown are  $K_i$ , <sup>2</sup> the values shown are  $IC_{50}$

#### 4.1.2. Protein Aggregation Inhibitors

The dysfunction and aggregation of A $\beta$  and tau proteins are the main features of AD pathology. A $\beta$  is a proteolytic product of amyloid precursor protein (APP), which is cleaved by  $\alpha$ -secretase and  $\gamma$ -secretase to A $\beta$  monomers with 38 to 43 amino acid residues, and studies have identified A $\beta_{42}$  as a key monomer in pathology [83,84]. These short A $\beta$  monomers possess a propensity to aggregate through mutual recognition to form A $\beta$  oligomers, which further aggregate into protofibrils and fibrils with a  $\beta$ -sheet conformation [85]. A $\beta$  has also shown a seeding effect in the brain to transmit and expand its influence [86].

Tau is a phosphoprotein, its hyperphosphorylation can destabilize microtubules, thus causing invariably compromised axonal transportation, synaptic dysfunction, and signal transmission failure [87]. Furthermore, hyperphosphorylated tau tends to congregate into paired helical filaments (PHFs) and straight filaments (SFs) in steps [88]. In experimental mouse models of tauopathy, the accumulation of aggregated tau can disrupt anterograde axonal transport and impair long-term potentiation [89,90].

In 2011, Hochdörffer et al. developed a series of A $\beta_{42}$  inhibitors based on a trimeric aminopyrazole carboxylic acid framework. They could convert well-ordered fibrils into less structured aggregates and thin bent filaments through backbone recognition and hydrophobic interactions with A $\beta_{42}$  (Figure 9) [91]. Compound (Trimer-TEG-Lys-OMe, **171**) displayed the most potent inhibition and disaggregation activities against fibril formation, with ~80% of reduced thioflavin fluorescence absorption and 43% of increased PC-12 cell viability in an A $\beta$  existing cytotoxic environment. Notably, the triethyleneglycol (TEG) spacer bridging trimeric aminopyrazole core and lysine appendix are essential to maintain the inhibition activity, as the spacer plays an active role in destabilizing the U-shaped turn of the A $\beta$  protofilament. When the spacer was omitted (**172**), an accelerated aggregation was contrarily observed. Meanwhile, the attached extension (TEG-Lys-OMe, **171**) allows diversity; when it was replaced by a pentapeptide "LPFFD", the corresponding new compound showed a substoichiometric  $IC_{50}$  value (3 μM). Considering that A $\beta$  concentration is at nanomolar range in the brain, much lower than the concentration (10 μM) used in in vitro studies, a 3 μM  $IC_{50}$  value is remarkable.

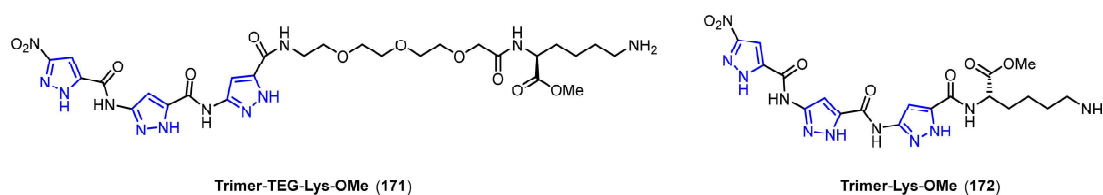


**Figure 9.** Chemical structures of pyrazole-containing  $A\beta_{42}$  inhibitors.

Anle138b (173) was first identified as a potent  $\alpha$ -synuclein aggregation inhibitor when it was administered in vivo at nanomolar concentrations [92]. Later in vitro and in vivo studies carried in mouse models of AD suggested that it could also inhibit the formation of pathological tau aggregates by specifically binding to pre-aggregated tau species [93]. Molecular dynamic (MD) simulations revealed that anle138b (173) could block the conversion of ordered antiparallel  $\beta$ -strands into disordered  $\beta$ -sheet rich conformations by preferentially interacting with pre-aggregated tau fragments to reduce the overall number of intermolecular hydrogen bonds [94]. Structure-activity analysis showed that the pyrazole scaffold plays a crucial role in anle138b's inhibitory effect; when the pyrazole moiety was replaced by imidazole (sery345, 174) or isoxazole (sery338, 175), the anti-aggregation effect was weakened due to altered hydrogen bond characteristics. Interestingly, pyrazole anle234b (176), a structural isomer of anle138b, is biologically inactive. Anle234b (176) is more sterically hindered than anle138b due to placement of the bulky bromine group at the ortho- rather than meta-position, which creates a more stable/less flexible conformation. The torsional inactivation of anle234b (176) hampers the interactions of the bromophenyl and pyrazole ring with peptide backbones, resulting in a reduced hydrogen bond strength (Figure 10) [92,94].

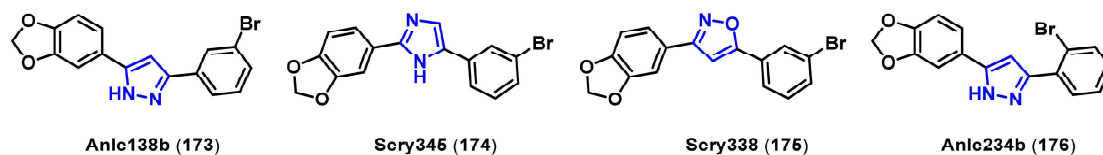


**Figure 10.** Chemical structures of pyrazole-containing inhibitors targeting tauopathy.

Curcumin (177), a natural phenolic compound found in the rhizome of *Curcuma longa*, has been used to treat various ailments in India for centuries. Structural modifications of curcumin to improve its instability and bioavailability have been an attractive strategy in new drug discovery [95,96]; several pyrazole-containing curcumin derivatives have showed potency for AD treatment [97]. CNB-001 (178), a pyrazole derivative of curcumin, was initially found to have broad neuroprotective activity [98,99]. Subsequent studies in AD animal models revealed that it could also promote  $A\beta$  clearance and improve memory [100]. Kotani et al. further found that CNB-001 (178) could stimulate the expression of the endoplasmic reticulum chaperone glucose-regulated protein 78 (GRP78) and increase formation of the amyloid precursor protein APP/GRP78 complex. The subsequent downregulation of intracellular APP trafficking results in a reduced  $A\beta$  production without inhibiting  $\beta$ - or  $\gamma$ -secretase activity [101]. Okuda et al. developed the inhibitor PE859 (179), this curcumin derivative has  $IC_{50}$  values of 1.2  $\mu$ M and 0.66  $\mu$ M, respectively, to inhibit  $A\beta$  and tau aggregations, and improved in vivo pharmacokinetics and pharmacological efficacy, making it is more competitive as an AD drug candidate than curcumin [102]. Furthermore, studies with PE859 (179) in the senescence-accelerated mouse prone 8 (SAMP8) model of accelerated aging showed it also protected cells from  $A\beta$ -induced cytotoxicity damage by decreasing  $A\beta$  and tau aggregations in the mouse brains (Figure 11) [103].

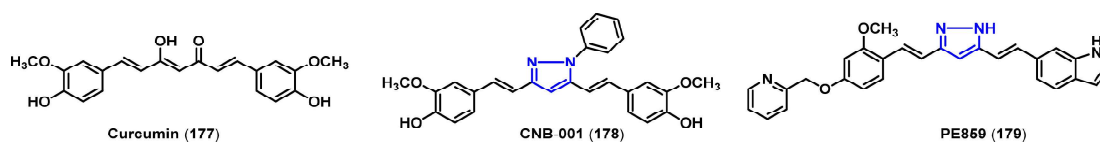


Figure 11. Chemical structures of pyrazole-containing curcumin derivatives.

#### 4.1.3. Phosphodiesterase (PDE) Inhibitors

Age-related cognitive decline and synaptic dysfunction are closely associated with decreased cAMP (cyclic guanosine monophosphate) and/or cGMP (cyclic guanosine monophosphate) concentration in the brains caused by increased phosphodiesterase (PDE) expression [104,105]. Therefore, PDE inhibitors that can specifically bind with high affinity to specific PDE isomers like PDE1, PDE5, or PDE9 to reduce the hydrolyzing of cAMP and/or cGMP have been evaluated for pharmaceutical potential in clinical trials for the treatment of AD [106].

The PDE1 group has three isoforms: PDE1A, 1B, and 1C, their activities are regulated by intracellular calcium and calmodulin (CaM) [104]. In human and rodent brains, PDE1A is predominantly expressed in the hippocampus, cortex, striatum, thalamus, and cerebellum; PDE1B is prevalent in the hippocampus, cortex, striatum; while PDE1C is more ubiquitously found in the cortex, cerebellum, and amygdala [107,108]. ITI214 (180), a potent and highly selective PDE1 inhibitor ( $K_i = 0.058$  nM), which is still in clinical trials, was developed by Intra-Cellular Therapies. This inhibitor was able to significantly enhance memory performance in vivo with a minimum effective dose of 3 mg/kg in various rat models (Figure 12) [109].

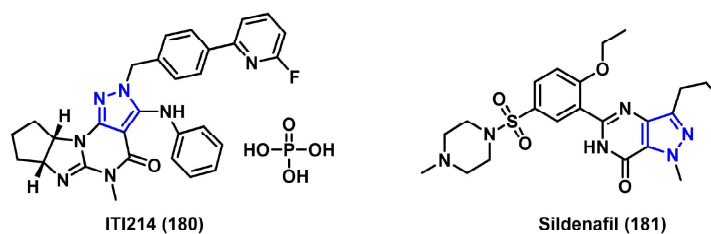


Figure 12. Chemical structures of pyrazole-containing PDE1 and PDE5 inhibitors.

The prominent expression of PDE5 in smooth muscles has led to the extraordinary success of PDE5 inhibitors including sildenafil (181), vardenafil, and tadalafil for the treatment of erectile dysfunction [105]. Furthermore, PDE5 is also expressed in human hippocampus and frontal cortex, and particularly abundant in Purkinje neurons [110,111]. Studies in different AD mouse models have indicated that sildenafil (181) can improve synaptic function, restore memory loss, and upregulate CREB phosphorylation signaling to reduce A $\beta$  levels over the long-term [112,113]. When administrated to anile Tg2576 transgenic mice (15 mg/kg, intraperitoneally), sildenafil (181) could completely reverse cognitive impairment and reduce tau hyperphosphorylation in the hippocampus [107]. More importantly, clinical trials of sildenafil (181) in healthy humans showed no central nervous system side effects. Although no overt effect on spatial auditory attention or visual word recognition was observed, sildenafil does help information processing and change specific components of event-related potentials with enhanced attention, and also reduced negativity of electroencephalogram in a memory task [114].

PDE9A is primarily expressed in the brain, with high concentrations in the cerebellum, neocortex, striatum, and hippocampus [115]. Consistent with the specific function of cGMP in controlling neurotransmission and enhancing hippocampal synaptic plasticity, the inhibition of PDE9A results in significant accumulation of cGMP in cerebrospinal fluid of nonhuman primates and humans, thus damaging brain functions like sensory processing, learning, and memory [116]. Compound PF-04447943 (182) ( $K_i = 8.3$  nM), a PDE9A inhibitor

developed by Pfizer, was found to increase cGMP concentration in cerebrospinal fluid by ~23-fold when dosed in rats, monkeys, and humans [117]. Unfortunately, no cognitive improvement was observed in subsequent phase II clinical trials when administered twice a day for 12 weeks to moderate stage AD patients. Instead, it resulted in a higher incidence of serious adverse events compared to the placebo group [118]. BI 409306 (**183**) is another potent PDE9A inhibitor, and has  $IC_{50}$  values of 65 nM and 168 nM in human and rat, respectively [119,120]. Preclinical studies demonstrated that BI 409306 (**183**) could increase cGMP concentrations in rodent prefrontal cortex and cerebrospinal fluid, and promoted long-term potentiation, and improved episodic and working memory performance [120]. Although it was well tolerated in prodromal to mild stage AD patients, its phase II clinical trial was discontinued because no visible efficacy in improving cognitive function was observed (Figure 13) [120].

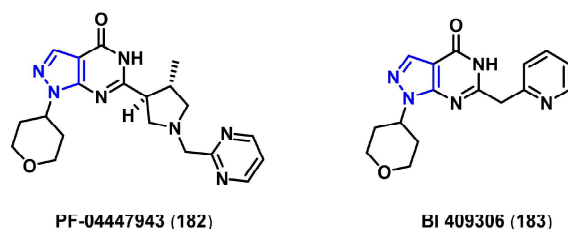


Figure 13. Chemical structures of pyrazole-containing PDE9 inhibitors.

#### 4.1.4. Dual Leucine Zipper Kinase (DLK) Inhibitors

Dual leucine zipper kinase (DLK, MAP3K12) mediates axon degeneration and neuronal apoptosis after activation [121]. DLK-inducible knockout mice displayed increased synaptic transmission and reduced neuronal degeneration when faced with neuronal insult [122]. Ex vivo imaging found that  $A\beta$ /plaque-associated synaptic loss is at least partially mediated by DLK signaling [123]. Experiments in mouse models of AD demonstrated that DLK deletion can reverse cognitive deficits and rescue certain phenotypical behaviors. Although the elimination of DLK did not reduce  $A\beta_{42}$  production, plaque load, or alter tau pathology, DLK-knockout mice had higher levels of full-length amyloid precursor protein (APP), amyloid plaque, plaque-associated gliosis, and enhanced cell survival in the subiculum of tau [123]. In 2015, Patel et al. reported the first small molecule DLK inhibitor **184** that effectively reduced c-Jun phosphorylation in nerve crush and 1-methyl-4-phenyl-1,2,3,6-tetrahydropyridine (MPTP)-induced neuronal injury [124]. The inhibitor **185** (DLK  $K_i = 42$  nM) was developed using a scaffold-hopping strategy, in which the pyrimidine core was replaced by a pyrazole; it exhibits comparable pharmacological properties and inhibitory activities to compound **184** in a rat model [125]. After further optimization, a more potent compound **186** (DLK  $K_i = 3$  nM) was identified. It had lower plasma clearance (total and unbound), a moderate volume of distribution, a long biological half-life, and good bioavailability when dosed in cynomolgus monkeys. A single dose of **186** ( $50 \text{ mg}\cdot\text{kg}^{-1}$ ) resulted in significantly decreased phosphorylation of c-Jun, leading to a near-complete inhibition of JNK when tested in a mouse model of AD (Figure 14) [126].

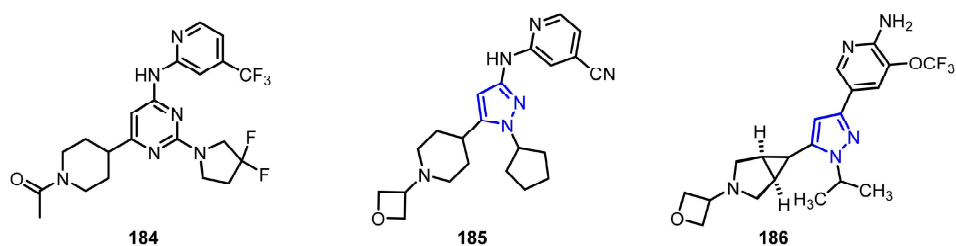


Figure 14. Chemical structures of pyrazole-containing dual leucine zipper kinase (DLK) inhibitors.

#### 4.1.5. Monoamine Oxidases B (MAO-B) Inhibitors

Monoamine oxidases (MAOs) are mitochondrial outer membrane-bound enzymes, existing as two distinct enzymatic isoforms, MAO-A and MAO-B, and are responsible for the metabolism of neurotransmitters such as dopamine, serotonin, adrenaline, and noradrenaline [127]. MAO-B inhibitors selegiline and rasagiline have been used to treat Parkinson's disease clinically. In addition, MAO-B inhibitors are also potential therapies for AD. A post-mortem brain study of AD cases indicated that MAO-B activity increased dramatically in three cortical regions (frontal, parietal, and occipital cortices), thalamus, and white matter [128], the observation was verified by another independent study [129]. MAO-B activity also increases in association with gliosis, resulting in elevated reactive oxygen species (ROS) levels, which in turn enhances A $\beta$  production by decreasing the activity of  $\alpha$ -secretase while enhancing the activity of  $\beta$ - and  $\gamma$ -secretases [130,131]. Studies suggest that MAO-B inhibitors like selegiline could slow AD progression in patients suffering from moderately severe impairment [132].

A new strategy for tackling the complexity of AD pathology is incorporating several pharmacological scaffolds into a single molecular entity to produce a synergistic effect [133]. This tactic turned out to be useful when fusing pharmacological scaffolds from a MAO-B inhibitor and an AChE inhibitor together to afford multi-target-directed lead compounds as potential therapeutics against AD [134,135]. Tzvetkov et al. reported three potent, reversible, and competitive MAO-B inhibitors (187–189) with high selectivity against the MAO-A isoform [136]. Enzyme studies suggest that all of them have the ability to bind to Fe(II) and Fe(III) via UV–Vis. These water-soluble, highly blood–brain barrier permeable MAO-B inhibitors are promising drug and radioligand candidates as diagnostic and therapeutic agents for AD (Figure 15, Table 2).

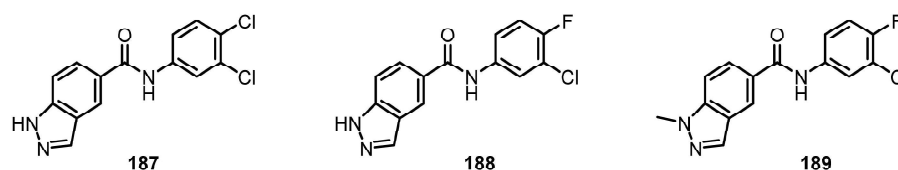


Figure 15. Chemical structures of monoamine oxidases (MAO) inhibitors.

Table 2. Affinities of monoamine oxidases B (MAO-B) inhibitors.

Compound	IC <sub>50</sub> Value (nM)			K <sub>i</sub> (nM)
	hMAO-A	hMAO-B	hMAO-A/hMAO-B	
187	>10,000	0.59 ± 0.09	>16,959	0.26 ± 0.04
188	>10,000	0.68 ± 0.04	>14,706	0.30 ± 0.02
189	≥10,000	0.66 ± 0.06	≥15,151	0.29 ± 0.03

#### 4.2. Applications of Pyrazoles in Parkinson's Disease (PD) Treatment

Parkinson's disease (PD) is the second most prevalent chronic neurodegenerative disease; it affects 1–2% of individuals over 60 years in the U.S. Initially, the most evident motor symptoms of PD are bradykinesia, muscle rigidity, and tremor; as the disease progresses, neurological symptoms including depression, pain, and sleep disturbance become more prevalent. Pyrazole derivatives have wide applications for PD treatment, and their roles can be divided into four classes: (1) antioxidants; (2) protein aggregation inhibitor; (3) adenosine A<sub>2A</sub> receptor antagonists; and (4) PDE10A inhibitors.

##### 4.2.1. Antioxidants

Mitochondrial dysfunction and subsequent oxidative stress are the main culprits leading to dopaminergic neuronal death in PD. Thus, antioxidants are potentially beneficial therapeutics in PD. Jayaraji and co-workers [137] reported that 2  $\mu$ M of CNB-001 (178)

could enhance cell viability insulted by reactive oxygen species (ROS). When applied to adult mice in a model of PD [137], CNB-001 (178) could significantly attenuate motor impairment, increase dopamine levels, and reduce inflammation. Two CNB-001 derivatives (190, 191) [138] are also promising therapeutic inhibitors for the treatment of PD caused by  $\alpha$ -synuclein amyloidosis, both of them have potent activity in preventing wide-type  $\alpha$ -synuclein aggregation and fibrilization, with two-fold higher activity than their isoxazole analogues (Figure 16) [138].

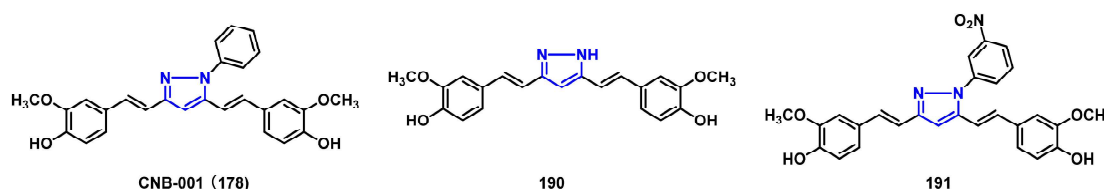


**Figure 16.** Chemical structures of pyrazole-containing antioxidants.

#### 4.2.2. Protein Aggregation Inhibitors

Anle138b (173) was first identified as a pharmaceutical candidate in inhibiting the aggregations of prion protein and of  $\alpha$ -synuclein [92]. In different mouse models of PD, anle138b (173) strongly inhibited  $\alpha$ -synuclein accumulation and neuronal degeneration and had an excellent oral bioavailability, while no detectable toxicity at therapeutic doses was observed [92]. When co-incubated with  $\alpha$ -synuclein fibrils, fluorescence spectrum indicated that it binds to the hydrophobic pockets of the fibril with good affinity ( $K_d = 190 \pm 120$  nM) (Figure 17) [139].

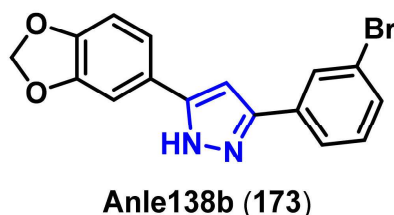


**Figure 17.** Chemical structure of a protein aggregation inhibitor.

#### 4.2.3. Adenosine Receptor $A_{2A}$ Receptor Antagonists

Adenosine receptor  $A_{2A}$  is abundantly expressed and co-localized with dopamine  $D_2$  in the striatum. The blockade of the  $A_{2A}$  receptor might antagonize dopaminergic neurotransmission in aspects relevant to motor control in PD patients [140], and the effect of  $A_{2A}$  antagonists has been supported by studies on rodent and primate PD models as well as preliminary clinical observations [141,142]. Pyrazole scaffolds have been widely employed in  $A_{2A}$  antagonists [143], for example, preladenant is discontinued due to lack of efficacy. Compound **192** [144] exhibited exceptional receptor binding affinity and ligand efficiency against adenosine  $A_{2A}$  receptor ( $K_i = 2.3$  nM), however, the 4-acetamide on the pyrimidine ring is unstable and tends to hydrolyze in acidic environments. To overcome this issue, a structurally stable compound **193** ( $K_i = 0.66$  nM) was optimized, unfortunately, it was subject to moderate cytochrome P450 (CYP) inhibition (80% inhibition of CYP3A4 at 10  $\mu$ M) [145]. Docking experiments based on crystal structure models of the adenosine receptor revealed that the 5-position of the pyrimidine ring was surrounded by multiple residues, which could serve as potential hydrogen bond donors or acceptors in the binding pocket. Analog **194**, which incorporated a cyano group, showed excellent potency and ligand efficiency with low cytochrome P450 inhibition [146]; when dosed orally as low as 3 mg/kg in rats, it could significantly reverse haloperidol-induced catalepsy (Figure 18).

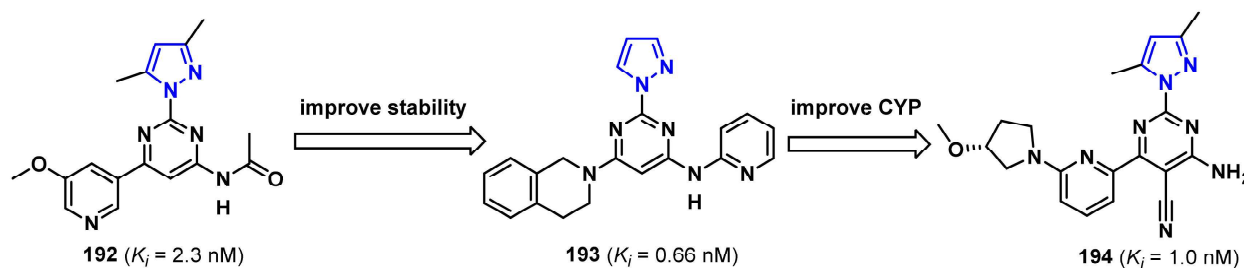


Figure 18. Chemical structures of pyrazole-containing  $A_{2A}$  receptor antagonists.

#### 4.2.4. Phosphodiesterase-10A (PDE10A) Enzyme Inhibitors

Phosphodiesterase 10A (PDE10A) is a dual substrate phosphodiesterase enzyme that can hydrolyze both cAMP and cGMP [139,147]. The PDE10A/cAMP interaction is essential for dopamine neurotransmission, and has been implicated in the pathophysiology of Parkinson's disease [148]. Investigators have reported that alteration of PDE10A expression is associated with progression and severity of patients with parkinsonism [149].

Tremendous effort has been dedicated to developing PDE10A inhibitors for the treatment of Parkinson's disease and other neuropsychiatric disorders characterized by regulating medial striatal neuron (MSN) activity. Meanwhile, selectivity of an inhibitor for PDE10A over the other subtypes is also a critical issue. Numerous studies indicate that inhibition of PDE3A/B can lead to arrhythmia and increased mortality [150]; PDE4 plays an important role as a regulator of central nervous system function while inhibition of PDE4A can increase heart and respiratory rates [151].

Among the multiple PDE10A inhibitors, 2-[4-(1-methyl-4-pyridin-4-yl-1H-pyrazol-3-yl)-phenoxy]methyl]-quinoline (MP-10) is highly potent ( $IC_{50} = 0.37$  nM), selective (>100-fold), and has been extensively evaluated as a therapeutic inhibitor. While MP-10 has progressed to clinical trials without success [152], other PDE10A analogues are under evaluation, though there is no currently FDA-approved PDE10A inhibitor for treating PD.

Tu et al. reported a series of structurally related analogues of MP-10 in which a methoxy group (-OCH<sub>3</sub>) was added into the 3-, 4-, or 6-position of the 2-methylquinoline moiety of the MP-10 pharmacophore (Figure 19) [153]. The most potent molecule was the 3- and 4-methoxy substituted quinolines (195) with an O atom bridge linkage that showed potency similar to MP-10. Interestingly, little difference was observed in the *in vitro* biological activity of regioisomer 196 (Table 3). More importantly, the six compounds 195a–c and 196a–c not only had high potency for PDE10A, but also high selectivity for PDE10A versus PDE3A/3B and 4A/4B (Table 3).

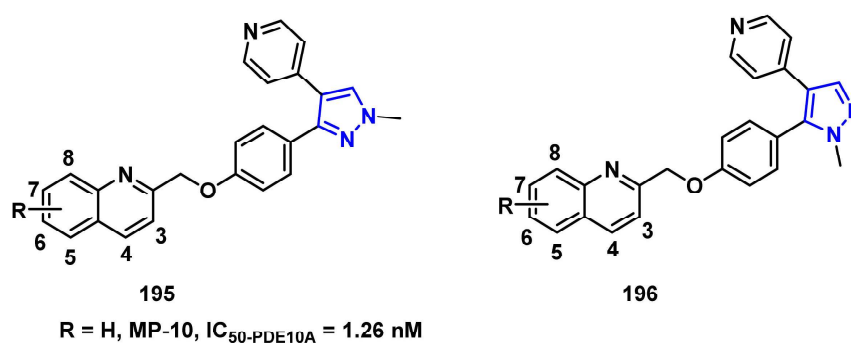
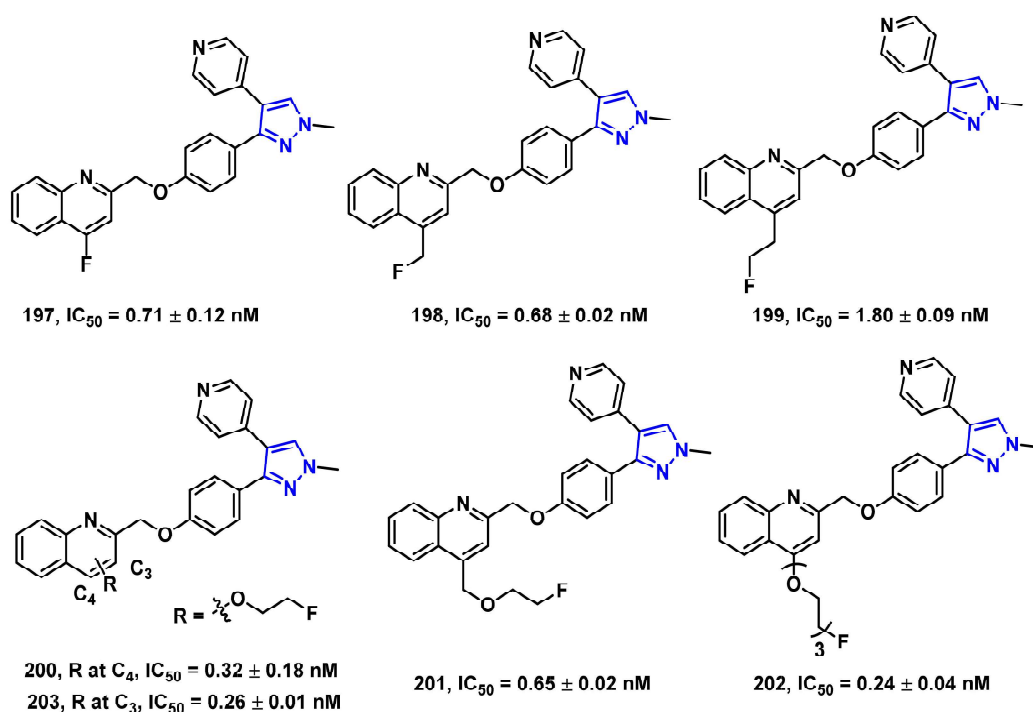


Figure 19. Chemical structures of pyrazole-containing PDE10A inhibitors.

**Table 3.** PDE affinities of new MP-10 analogues.

Compound	R	IC <sub>50</sub> Value				
		PDE10A (nM)	PDE3A (10 <sup>3</sup> × nM)	PDE3B (10 <sup>3</sup> × nM)	PDE4A (10 <sup>3</sup> × nM)	PDE4B (10 <sup>3</sup> × nM)
195a	3-OMe	0.40 ± 0.02	123 ± 21	82.7 ± 10	3.85 ± 0.23	3.43 ± 0.21
195b	4-OMe	0.28 ± 0.06	27.5 ± 2.5	3.85 ± 0.95	2.56 ± 0.11	1.79 ± 0.10
195c	6-OMe	1.82 ± 0.25	78.0 ± 4.0	9.75 ± 1.25	3.37 ± 0.18	2.56 ± 0.09
196a	3-OMe	0.24 ± 0.05	18.7 ± 3.1	16.9 ± 2.1	199 ± 16.0	31.5 ± 3.60
196b	4-OMe	0.36 ± 0.03	29.0 ± 4.0	4.80 ± 1.20	4.18 ± 0.33	5.06 ± 0.40
196c	6-OMe	1.78 ± 0.03	1.5 ± 0.5	3.00 ± 0.14	5.60 ± 0.52	7.10 ± 0.58

In 2015, another series of potent and selective PDE10A inhibitors were reported by Tu et al. [154] (Figure 20). Fluorine-containing groups were introduced into the 2-methylquinoline moiety of MP-10. These new potent compounds (197–202) (IC<sub>50</sub> range 0.24–1.80 nM) had >210-fold selectivity.

**Figure 20.** Structures of potent fluorine-containing MP-10 analogues.

## 5. Conclusions

The wide applications of pyrazoles in pharmaceuticals have stimulated the rapid methodological development of pyrazole synthesis. During the past decade, many general and practical approaches including the involvement of transition-metal catalysts, photoredox reactions, one-pot multicomponent process, new reactants, and novel reaction type have led to fruitful advances in the fields of the synthesis and functionalization of pyrazole derivatives. This review briefly covers these updates, and highlights the potential of pyrazole scaffolds in pharmaceutical development for AD and PD treatment, two of the most serious chronic neurodegenerative diseases. The varied pyrazole compounds described herein can be regarded as candidate agents for the development of novel neurodegenerative drugs. Although in vitro and in vivo studies with promising therapeutics have shown potential to alleviate neurodegenerative symptoms, they are still far from providing a cure or effective treatment, largely due to a lack of clear understanding of



disease pathologies. Therefore, studies based on rational drug design and that incorporate a deep understanding of pathological changes in neurodegenerative disease are urgently needed to explore the potential utility of pyrazoles as therapeutics, and this effort relies on multidisciplinary cooperation ranging from medicinal chemistry to pathophysiology.

**Author Contributions:** Conceptualization, Z.T. and X.L.; Software, Writing—original draft preparation, X.L.; Writing—review and editing, Z.T., X.L., and Y.Y.; Visualization, X.L. and Y.Y.; Supervision, Z.T.; Funding acquisition, Z.T. All authors have read and agreed to the published version of the manuscript.

**Funding:** The authors received financial support from the USA National Institutes of Health (NS075527, NS103957, NS103988, U19NS110456).

**Acknowledgments:** The authors also thank Lynne Jones for assistance with the manuscript.

**Conflicts of Interest:** The authors declare no conflict of interest.

## References

1. Giornal, F.; Pazenok, S.; Rodefeld, L.; Lui, N.; Vors, J.P.; Leroux, F.R. Synthesis of diversely fluorinated pyrazoles as novel active agrochemical ingredients. *J. Fluorine Chem.* **2013**, *152*, 2–11. [[CrossRef](#)]
2. Khan, M.F.; Alam, M.M.; Verma, G.; Akhtar, W.; Akhter, M.; Shaquiquzzaman, M. The therapeutic voyage of pyrazole and its analogs: A review. *Eur. J. Med. Chem.* **2016**, *120*, 170–201. [[CrossRef](#)] [[PubMed](#)]
3. Karrouchi, K.; Radi, S.; Ramli, Y.; Taoufik, J.; Mabkhot, Y.N.; Al-Aizari, F.A.; Ansar, M. Synthesis and pharmacological activities of pyrazole derivatives: A review. *Molecules* **2018**, *23*, 134. [[CrossRef](#)] [[PubMed](#)]
4. Byon, W.; Garonzik, S.; Boyd, R.A.; Frost, C.E. Apixaban: A clinical pharmacokinetic and pharmacodynamic review. *Clin. Pharmacokinet.* **2019**, *58*, 1265–1279. [[CrossRef](#)] [[PubMed](#)]
5. Fustero, S.; Sanchez-Rosello, M.; Barrio, P.; Simon-Fuentes, A. From 2000 to mid-2010: A fruitful decade for the synthesis of pyrazoles. *Chem. Rev.* **2011**, *111*, 6984–7034. [[CrossRef](#)]
6. Gomes, P.M.O.; Silva, A.M.S.; Silva, V.L.M. Pyrazoles as key scaffolds for the development of fluorine-18-labeled radiotracers for positron emission tomography (PET). *Molecules* **2020**, *25*, 1722. [[CrossRef](#)]
7. Turkan, F.; Cetin, A.; Taslimi, P.; Gulcin, I. Some pyrazoles derivatives: Potent carbonic anhydrase,  $\alpha$ -glycosidase, and cholinesterase enzymes inhibitors. *Arch. Pharm.* **2018**, *351*, e1800200. [[CrossRef](#)]
8. Hazarika, R.; Konwar, M.; Damarla, K.; Kumar, A.; Sarma, D. HBF<sub>4</sub>/ACN: A simple and efficient protocol for the synthesis of pyrazoles under ambient reaction conditions. *Synth. Commun.* **2019**, *50*, 329–337. [[CrossRef](#)]
9. Wang, H.F.; Sun, X.L.; Zhang, S.L.; Liu, G.L.; Wang, C.J.; Zhu, L.L.; Zhang, H. Efficient copper-catalyzed synthesis of substituted pyrazoles at room temperature. *Synlett* **2018**, *29*, 2689–2692. [[CrossRef](#)]
10. Kumar, S.V.; Yadav, S.K.; Raghava, B.; Saraiah, B.; Ila, H.; Rangappa, K.S.; Hazra, A. Cyclocondensation of arylhydrazines with 1,3-bis(het)arylmonothio-1,3-diketones and 1,3-bis(het)aryl-3-(methylthio)-2-propenones: Synthesis of 1-aryl-3,5-bis(het)arylpyrazoles with complementary regioselectivity. *J. Org. Chem.* **2013**, *78*, 4960–4973. [[CrossRef](#)] [[PubMed](#)]
11. Schmitt, D.C.; Taylor, A.P.; Flick, A.C.; Kyne, R.E., Jr. Synthesis of pyrazoles from 1,3-diols via hydrogen transfer catalysis. *Org. Lett.* **2015**, *17*, 1405–1408. [[CrossRef](#)] [[PubMed](#)]
12. Zhang, X.; Kang, J.; Niu, P.; Wu, J.; Yu, W.; Chang, J. I<sub>2</sub>-mediated oxidative C-N bond formation for metal-free one-pot synthesis of di-, tri-, and tetrasubstituted pyrazoles from  $\alpha,\beta$ -unsaturated aldehydes/ketones and hydrazines. *J. Org. Chem.* **2014**, *79*, 10170–10178. [[CrossRef](#)] [[PubMed](#)]
13. Gutti, G.; Kumar, D.; Paliwal, P.; Ganeshpurkar, A.; Lahre, K.; Kumar, A.; Krishnamurthy, S.; Singh, S.K. Development of pyrazole and spiropyrazoline analogs as multifunctional agents for treatment of Alzheimer's disease. *Bioorg. Chem.* **2019**, *90*, 103080. [[CrossRef](#)] [[PubMed](#)]
14. Ding, Y.; Zhang, T.; Chen, Q.Y.; Zhu, C. Visible-light photocatalytic aerobic annulation for the green synthesis of pyrazoles. *Org. Lett.* **2016**, *18*, 4206–4209. [[CrossRef](#)]
15. Hu, J.; Chen, S.; Sun, Y.; Yang, J.; Rao, Y. Synthesis of tri- and tetrasubstituted pyrazoles via Ru(II) catalysis: Intramolecular aerobic oxidative C-N coupling. *Org. Lett.* **2012**, *14*, 5030–5033. [[CrossRef](#)]
16. Harigae, R.; Moriyama, K.; Togo, H. Preparation of 3,5-disubstituted pyrazoles and isoxazoles from terminal alkynes, aldehydes, hydrazines, and hydroxylamine. *J. Org. Chem.* **2014**, *79*, 2049–2058. [[CrossRef](#)] [[PubMed](#)]
17. Raji Reddy, C.; Vijaykumar, J.; Grée, R. Facile one-pot synthesis of 3,5-disubstituted 1H-pyrazoles from propargylic alcohols via propargyl hydrazides. *Synthesis* **2013**, *45*, 830–836. [[CrossRef](#)]
18. Guo, Y.; Wang, G.; Wei, L.; Wan, J.P. Domino C-H sulfonylation and pyrazole annulation for fully substituted pyrazole synthesis in water using hydrophilic enamines. *J. Org. Chem.* **2019**, *84*, 2984–2990. [[CrossRef](#)] [[PubMed](#)]
19. Raghunadh, A.; Meruva, S.B.; Mekala, R.; Rao, K.R.; Krishna, T.; Chary, R.G.; Rao, L.V.; Kumar, U.K.S. An efficient regioselective copper catalyzed multi-component synthesis of 1,3-disubstituted pyrazoles. *Tetrahedron Lett.* **2014**, *55*, 2986–2990. [[CrossRef](#)]

20. Chen, J.; Properzi, R.; Uccello, D.P.; Young, J.A.; Dushin, R.G.; Starr, J.T. One-pot oxidation and rearrangement of propargylamines and in situ pyrazole synthesis. *Org. Lett.* **2014**, *16*, 4146–4149. [[CrossRef](#)] [[PubMed](#)]
21. Tang, M.; Zhang, F.M. Efficient one-pot synthesis of substituted pyrazoles. *Tetrahedron* **2013**, *69*, 1427–1433. [[CrossRef](#)]
22. Wen, J.; Fu, Y.; Zhang, R.Y.; Zhang, J.; Chen, S.Y.; Yu, X.Q. A simple and efficient synthesis of pyrazoles in water. *Tetrahedron* **2011**, *67*, 9618–9621. [[CrossRef](#)]
23. Zhang, G.; Ni, H.; Chen, W.; Shao, J.; Liu, H.; Chen, B.; Yu, Y. One-pot three-component approach to the synthesis of polyfunctional pyrazoles. *Org. Lett.* **2013**, *15*, 5967–5969. [[CrossRef](#)]
24. Sha, Q.; Wei, Y.Y. An efficient one-pot synthesis of 3,5-diaryl-4-bromopyrazoles by 1,3-dipolar cycloaddition of in situ generated diazo compounds and 1-bromoalk-1-ynes. *Synthesis* **2013**, *45*, 413–420. [[CrossRef](#)]
25. Wang, L.; Huang, J.; Gong, X.; Wang, J. Highly regioselective organocatalyzed synthesis of pyrazoles from diazoacetates and carbonyl compounds. *Chem. Eur. J.* **2013**, *19*, 7555–7560. [[CrossRef](#)]
26. Jackowski, O.; Lecourt, T.; Micouin, L. Direct synthesis of polysubstituted aluminosoxazoles and pyrazoles by a metalative cyclization. *Org. Lett.* **2011**, *13*, 5664–5667. [[CrossRef](#)]
27. Li, D.Y.; Mao, X.F.; Chen, H.J.; Chen, G.R.; Liu, P.N. Rhodium-catalyzed addition-cyclization of hydrazines with alkynes: Pyrazole synthesis via unexpected C-N bond cleavage. *Org. Lett.* **2014**, *16*, 3476–3479. [[CrossRef](#)]
28. Ledovskaya, M.S.; Voronin, V.V.; Polynski, M.V.; Lebedev, A.N.; Ananikov, V.P. Primary vinyl ethers as acetylene surrogate: A flexible tool for deuterium-labeled pyrazole synthesis. *Eur. J. Org. Chem.* **2020**, *2020*, 4571–4580. [[CrossRef](#)]
29. Kobayashi, E.; Togo, H. Facile one-pot transformation of primary alcohols into 3-aryl- and 3-alkyl-isoxazoles and -pyrazoles. *Synthesis* **2019**, *51*, 3723–3735. [[CrossRef](#)]
30. Panda, N.; Jena, A.K. Fe-catalyzed one-pot synthesis of 1,3-di- and 1,3,5-trisubstituted pyrazoles from hydrazones and vicinal diols. *J. Org. Chem.* **2012**, *77*, 9401–9406. [[CrossRef](#)] [[PubMed](#)]
31. Fan, X.W.; Lei, T.; Zhou, C.; Meng, Q.Y.; Chen, B.; Tung, C.H.; Wu, L.Z. Radical addition of hydrazones by  $\alpha$ -bromo ketones to prepare 1,3,5-trisubstituted pyrazoles via visible light catalysis. *J. Org. Chem.* **2016**, *81*, 7127–7133. [[CrossRef](#)]
32. Yi, F.; Zhao, W.; Wang, Z.; Bi, X. Silver-mediated [3+2] cycloaddition of alkynes and N-isocyanoiminotriphenylphosphorane: Access to monosubstituted pyrazoles. *Org. Lett.* **2019**, *21*, 3158–3161. [[CrossRef](#)]
33. Zhu, J.N.; Wang, W.K.; Jin, Z.H.; Wang, Q.K.; Zhao, S.Y. Pyrrolo[3,4-c]pyrazole synthesis via copper(I) chloride-catalyzed oxidative coupling of hydrazones to maleimides. *Org. Lett.* **2019**, *21*, 5046–5050. [[CrossRef](#)]
34. Specklin, S.; Decuypere, E.; Plougastel, L.; Aliani, S.; Taran, F. One-pot synthesis of 1,4-disubstituted pyrazoles from arylglycines via copper-catalyzed sydnone-alkyne cycloaddition reaction. *J. Org. Chem.* **2014**, *79*, 7772–7777. [[CrossRef](#)]
35. Lakeland, C.P.; Watson, D.W.; Harrity, J.P.A. Exploiting synergistic catalysis for an ambient temperature photocycloaddition to pyrazoles. *Chem. Eur. J.* **2020**, *26*, 155–159. [[CrossRef](#)] [[PubMed](#)]
36. Zhang, Q.; Meng, L.G.; Wang, K.; Wang, L. nBu<sub>3</sub>P-catalyzed desulfonylative [3 + 2] cycloadditions of allylic carbonates with arylazosulfones to pyrazole derivatives. *Org. Lett.* **2015**, *17*, 872–875. [[CrossRef](#)] [[PubMed](#)]
37. Zhang, Y.C.; Liu, J.; Jia, X.S. Phosphine-free [3+2] cycloaddition of propargylamines with dialkyl azodicarboxylates: An efficient access to pyrazole backbone. *Synthesis* **2018**, *50*, 3499–3505.
38. Pearce, A.J.; Harkins, R.P.; Reiner, B.R.; Wotal, A.C.; Dunscomb, R.J.; Tonks, I.A. Multicomponent pyrazole synthesis from alkynes, nitriles, and titanium imido complexes via oxidatively induced N-N bond coupling. *J. Am. Chem. Soc.* **2020**, *142*, 4390–4399. [[CrossRef](#)]
39. Sloop, J.C.; Holder, C.; Henary, M. Selective incorporation of fluorine in pyrazoles. *Eur. J. Org. Chem.* **2015**, *2015*, 3405–3422. [[CrossRef](#)]
40. Prieto, A.; Bouyssi, D.; Monteiro, N. Ruthenium-catalyzed tandem C-H fluoromethylation/cyclization of N-alkylhydrazones with CBr<sub>3</sub>F: Access to 4-fluoropyrazoles. *J. Org. Chem.* **2017**, *82*, 3311–3316. [[CrossRef](#)]
41. Schmitt, E.; Panossian, A.; Vors, J.P.; Funke, C.; Lui, N.; Pazenok, S.; Leroux, F.R. A major advance in the synthesis of fluoroalkyl pyrazoles: Tuneable regioselectivity and broad substitution patterns. *Chem. Eur. J.* **2016**, *22*, 11239–11244. [[CrossRef](#)] [[PubMed](#)]
42. Schmitt, E.; Bouvet, S.; Pegot, B.; Panossian, A.; Vors, J.P.; Pazenok, S.; Magnier, E.; Leroux, F.R. Fluoroalkyl amino reagents for the introduction of the fluoro(trifluoromethoxy)methyl group onto arenes and heterocycles. *Org. Lett.* **2017**, *19*, 4960–4963. [[CrossRef](#)] [[PubMed](#)]
43. Mykhailiuk, P.K. In situ generation of difluoromethyl diazomethane for [3+2] cycloadditions with alkynes. *Angew. Chem. Int. Ed.* **2015**, *54*, 6558–6561. [[CrossRef](#)] [[PubMed](#)]
44. Montoya, V.; Pons, J.; García-Antón, J.; Solans, X.; Font-Bardia, M.; Ros, J. Reaction of 2-hydroxyethylhydrazine with a trifluoromethyl- $\beta$ -diketone: Study and structural characterization of a new 5-hydroxy-5-trifluoromethyl-4,5-dihydropyrazole intermediate. *J. Fluorine Chem.* **2007**, *128*, 1007–1011. [[CrossRef](#)]
45. Li, F.; Nie, J.; Sun, L.; Zheng, Y.; Ma, J.A. Silver-mediated cycloaddition of alkynes with CF<sub>3</sub>CHN<sub>2</sub>: Highly regioselective synthesis of 3-trifluoromethylpyrazoles. *Angew. Chem. Int. Ed.* **2013**, *52*, 6255–6258. [[CrossRef](#)] [[PubMed](#)]
46. Sun, A.; Chandrakumar, N.; Yoon, J.-J.; Plemper, R.K.; Snyder, J.P. Non-nucleoside inhibitors of the measles virus RNA-dependent RNA polymerase complex activity: Synthesis and in vitro evaluation. *Bioorg. Med. Chem. Lett.* **2007**, *17*, 5199–5203. [[CrossRef](#)]
47. Ji, G.; Wang, X.; Zhang, S.; Xu, Y.; Ye, Y.; Li, M.; Zhang, Y.; Wang, J. Synthesis of 3-trifluoromethylpyrazoles via trifluoromethylation/cyclization of  $\alpha,\beta$ -alkynic hydrazones using a hypervalent iodine reagent. *Chem. Commun.* **2014**, *50*, 4361–4363. [[CrossRef](#)]
48. Liu, H.; Laforest, R.; Gu, J.; Luo, Z.; Jones, L.A.; Gropler, R.J.; Benzinger, T.L.S.; Tu, Z. Acute rodent tolerability, toxicity, and radiation dosimetry estimates of the S1P1-specific radioligand [<sup>11</sup>C]CS<sub>1</sub>P<sub>1</sub>. *Mol. Imaging. Biol.* **2020**, *22*, 285–292. [[CrossRef](#)] [[PubMed](#)]

49. Wang, Q.; He, L.; Li, K.K.; Tsui, G.C. Copper-mediated domino cyclization/trifluoromethylation/deprotection with TMSCF<sub>3</sub>: Synthesis of 4-(trifluoromethyl)pyrazoles. *Org. Lett.* **2017**, *19*, 658–661. [[CrossRef](#)]
50. Trofymchuk, S.; Bugera, M.Y.; Klipkov, A.A.; Razhyk, B.; Semenov, S.; Tarasenko, K.; Starova, V.S.; Zaporozhets, O.A.; Tananaiko, O.Y.; Alekseenko, A.N.; et al. Deoxofluorination of (hetero)aromatic acids. *J. Org. Chem.* **2020**, *85*, 3110–3124. [[CrossRef](#)] [[PubMed](#)]
51. Dhanju, S.; Caravana, A.C.; Thomson, R.J. Access to  $\alpha$ -pyrazole and  $\alpha$ -triazole derivatives of ketones from oxidative heteroarylation of silyl enolethers. *Org. Lett.* **2020**, *22*, 8055–8058. [[CrossRef](#)] [[PubMed](#)]
52. Kumar, V.; Kaur, K.; Gupta, G.K.; Sharma, A.K. Pyrazole containing natural products: Synthetic preview and biological significance. *Eur. J. Med. Chem.* **2013**, *69*, 735–753. [[CrossRef](#)]
53. Luo, G.; Chen, L. Gold-catalyzed stereoselective 1,4-conjugate addition of pyrazoles to propiolates and their hydrogenation to  $\beta$ -pyrazolyl acid esters. *Tetrahedron Lett.* **2015**, *56*, 6276–6278. [[CrossRef](#)]
54. Roughley, S.D.; Jordan, A.M. The medicinal chemist's toolbox: An analysis of reactions used in the pursuit of drug candidates. *J. Med. Chem.* **2011**, *54*, 3451–3479. [[CrossRef](#)] [[PubMed](#)]
55. Viciano-Chumillas, M.; Tanase, S.; de Jongh, L.J.; Reedijk, J. Coordination versatility of pyrazole-based ligands towards high-nuclearity transition-metal and rare-earth clusters. *Eur. J. Inorg. Chem.* **2010**, *2010*, 3403–3418. [[CrossRef](#)]
56. Ruiz-Castillo, P.; Buchwald, S.L. Applications of palladium-catalyzed C-N cross-coupling reactions. *Chem. Rev.* **2016**, *116*, 12564–12649. [[CrossRef](#)]
57. Ma, D.; Cai, Q.; Zhang, H. Mild method for Ullmann coupling reaction of amines and aryl halides. *Org. Lett.* **2003**, *5*, 2453–2455. [[CrossRef](#)] [[PubMed](#)]
58. Onodera, S.; Kochi, T.; Kakiuchi, F. Synthesis of N-arylpiprazoles by palladium-catalyzed coupling of aryl triflates with pyrazole derivatives. *J. Org. Chem.* **2019**, *84*, 6508–6515. [[CrossRef](#)]
59. Zhou, Q.; Du, F.; Chen, Y.; Fu, Y.; Sun, W.; Wu, Y.; Chen, G. L-(-)-Quebrachitol as a ligand for selective copper(0)-catalyzed N-arylation of nitrogen-containing heterocycles. *J. Org. Chem.* **2019**, *84*, 8160–8167. [[CrossRef](#)] [[PubMed](#)]
60. Cristau, H.-J.; Cellier, P.P.; Spindler, J.-F.; Taillefer, M. Mild conditions for copper-catalysed N-arylation of pyrazoles. *Eur. J. Org. Chem.* **2004**, *2004*, 695–709. [[CrossRef](#)]
61. Wang, J.; Li, J.H.; Guo, Y.; Dong, H.; Liu, Q.; Yu, X.Q. TEMPO-mediated C-H amination of benzoxazoles with N-heterocycles. *J. Org. Chem.* **2020**, *85*, 12797–12803. [[CrossRef](#)]
62. Aggarwal, R.; Kumar, V.; Kumar, R.; Singh, S.P. Approaches towards the synthesis of 5-aminopyrazoles. *Beilstein J. Org. Chem.* **2011**, *7*, 179–197. [[CrossRef](#)] [[PubMed](#)]
63. Senadi, G.C.; Hu, W.P.; Lu, T.Y.; Garkhedkar, A.M.; Vandavasi, J.K.; Wang, J.J. I<sub>2</sub>-TBHP-catalyzed oxidative cross-coupling of N-sulfonyl hydrazones and isocyanides to 5-aminopyrazoles. *Org. Lett.* **2015**, *17*, 1521–1524. [[CrossRef](#)]
64. Kallman, N.J.; Cole, K.P.; Koenig, T.M.; Buser, J.Y.; McFarland, A.D.; McNulty, L.M.; Mitchell, D. Synthesis of aminopyrazoles from isoxazoles: Comparison of preparative methods by in situ NMR analysis. *Synthesis* **2016**, *48*, 3537–3543.
65. Soriano-Garcia, M. Organoselenium compounds as potential therapeutic and chemopreventive agents: A review. *Curr. Med. Chem.* **2004**, *11*, 1657–1669. [[CrossRef](#)] [[PubMed](#)]
66. Gandin, V.; Khalkar, P.; Braude, J.; Fernandes, A.P. Organic selenium compounds as potential chemotherapeutic agents for improved cancer treatment. *Free Radic. Biol. Med.* **2018**, *127*, 80–97. [[CrossRef](#)]
67. Desai, D.; Kaushal, N.; Gandhi, U.H.; Arner, R.J.; D'Souza, C.; Chen, G.; Vunta, H.; El-Bayoumy, K.; Amin, S.; Prabhu, K.S. Synthesis and evaluation of the anti-inflammatory properties of selenium-derivatives of celecoxib. *Chem. Biol. Interact.* **2010**, *188*, 446–456. [[CrossRef](#)] [[PubMed](#)]
68. Belladonna, A.L.; Cervo, R.; Alves, D.; Barcellos, T.; Cargnelutti, R.; Schumacher, R.F. C-H functionalization of (hetero)arenes: Direct selenylation mediated by Selectfluor. *Tetrahedron Lett.* **2020**, *61*, 152035. [[CrossRef](#)]
69. Wang, X.; Liu, W.G.; Tung, C.H.; Wu, L.Z.; Cong, H. A monophosphine ligand derived from anthracene photodimer: Synthetic applications for palladium-catalyzed coupling reactions. *Org. Lett.* **2019**, *21*, 8158–8163. [[CrossRef](#)]
70. Kirsten, C.N.; Schrader, T.H. Intermolecular  $\beta$ -sheet stabilization with aminopyrazoles. *J. Am. Chem. Soc.* **1997**, *119*, 12061–12068. [[CrossRef](#)]
71. Rzepecki, P.; Schrader, T.  $\beta$ -Sheet ligands in action: KLVFF recognition by aminopyrazole hybrid receptors in water. *J. Am. Chem. Soc.* **2005**, *127*, 3016–3025. [[CrossRef](#)] [[PubMed](#)]
72. Frisoni, G.B.; Laakso, M.P.; Beltramello, A.; Geroldi, C.; Bianchetti, A.; Soinenen, H.; Trabucchi, M. Hippocampal and entorhinal cortex atrophy in frontotemporal dementia and Alzheimer's disease. *Neurology* **1999**, *52*, 91–100. [[CrossRef](#)]
73. Hardy, J.A.; Higgins, G.A. Alzheimer's disease: The amyloid cascade hypothesis. *Science* **1992**, *256*, 184–185. [[CrossRef](#)] [[PubMed](#)]
74. Savelieff, M.G.; Nam, G.; Kang, J.; Lee, H.J.; Lee, M.; Lim, M.H. Development of multifunctional molecules as potential therapeutic candidates for Alzheimer's disease, Parkinson's disease, and amyotrophic lateral sclerosis in the last decade. *Chem. Rev.* **2019**, *119*, 1221–1322. [[CrossRef](#)]
75. Francis, P.T.; Palmer, A.M.; Snape, M.; Wilcock, G.K. The cholinergic hypothesis of Alzheimer's disease: A review of progress. *J. Neurol. Neurosurg. Psychiatry* **1999**, *66*, 137–147. [[CrossRef](#)] [[PubMed](#)]
76. Fonnum, F. Radiochemical micro assays for the determination of choline acetyltransferase and acetylcholinesterase activities. *Biochem. J.* **1969**, *115*, 465–472. [[CrossRef](#)] [[PubMed](#)]
77. Lockridge, O. Review of human butyrylcholinesterase structure, function, genetic variants, history of use in the clinic, and potential therapeutic uses. *Pharmacol. Ther.* **2015**, *148*, 34–46. [[CrossRef](#)]

78. Bartolini, M.; Bertucci, C.; Cavrini, V.; Andrisano, V.  $\beta$ -Amyloid aggregation induced by human acetylcholinesterase: Inhibition studies. *Biochem. Pharmacol.* **2003**, *65*, 407–416. [[CrossRef](#)]
79. Greig, N.H.; Utsuki, T.; Ingram, D.K.; Wang, Y.; Pepeu, G.; Scali, C.; Yu, Q.S.; Mamczarz, J.; Holloway, H.W.; Giordano, T.; et al. Selective butyrylcholinesterase inhibition elevates brain acetylcholine, augments learning and lowers Alzheimer  $\beta$ -amyloid peptide in rodent. *Proc. Natl. Acad. Sci. USA* **2005**, *102*, 17213–17218. [[CrossRef](#)]
80. Nordberg, A.; Ballard, C.; Bullock, R.; Darreh-Shori, T.; Somogyi, M. A review of butyrylcholinesterase as a therapeutic target in the treatment of Alzheimer's disease. *Prim. Care. Companion CNS Disord.* **2013**, *15*. [[CrossRef](#)]
81. Shaikh, S.; Dhavan, P.; Pavale, G.; Ramana, M.M.V.; Jadhav, B.L. Design, synthesis and evaluation of pyrazole bearing  $\alpha$ -aminophosphonate derivatives as potential acetylcholinesterase inhibitors against Alzheimer's disease. *Bioorg. Chem.* **2020**, *96*, 103589–103611. [[CrossRef](#)] [[PubMed](#)]
82. Silva, D.; Chioua, M.; Samadi, A.; Carmo Carreiras, M.; Jimeno, M.L.; Mendes, E.; Rios Cde, L.; Romero, A.; Villarroya, M.; Lopez, M.G.; et al. Synthesis and pharmacological assessment of diversely substituted pyrazolo[3,4-*b*]quinoline, and benzo[*b*]pyrazolo[4,3-*g*][1,8]naphthyridine derivatives. *Eur. J. Med. Chem.* **2011**, *46*, 4676–4681. [[CrossRef](#)]
83. Esch, F.S.; Keim, P.S.; Beattie, E.C.; Blacher, R.W.; Culwell, A.R.; Oltersdorf, T.; McClure, D.; Ward, P.J. Cleavage of amyloid beta peptide during constitutive processing of its precursor. *Science* **1990**, *248*, 1122–1124. [[CrossRef](#)] [[PubMed](#)]
84. Zhang, Y.W.; Thompson, R.; Zhang, H.; Xu, H. APP processing in Alzheimer's disease. *Mol. Brain* **2011**, *4*, 3–15. [[CrossRef](#)] [[PubMed](#)]
85. Lee, S.J.; Nam, E.; Lee, H.J.; Savelieff, M.G.; Lim, M.H. Towards an understanding of amyloid- $\beta$  oligomers: Characterization, toxicity mechanisms, and inhibitors. *Chem. Soc. Rev.* **2017**, *46*, 310–323. [[CrossRef](#)]
86. Kane, M.D.; Lipinski, W.J.; Callahan, M.J.; Bian, F.; Durham, R.A.; Schwarz, R.D.; Roher, A.E.; Walker, L.C. Evidence for seeding of  $\beta$ -amyloid by intracerebral infusion of Alzheimer brain extracts in  $\beta$ -amyloid precursor protein-transgenic mice. *J. Neurosci.* **2000**, *20*, 3606–3611. [[CrossRef](#)]
87. Ballatore, C.; Lee, V.M.; Trojanowski, J.Q. Tau-mediated neurodegeneration in Alzheimer's disease and related disorders. *Nat. Rev. Neurosci.* **2007**, *8*, 663–672. [[CrossRef](#)]
88. Grundke-Iqbal, I.; Iqbal, K.; Tung, Y.C.; Quinlan, M.; Wisniewski, H.M.; Binder, L.I. Abnormal phosphorylation of the microtubule-associated protein  $\tau$  (tau) in Alzheimer cytoskeletal pathology. *Proc. Natl. Acad. Sci. USA* **1986**, *83*, 4913–4917. [[CrossRef](#)] [[PubMed](#)]
89. Polydoro, M.; Acker, C.M.; Duff, K.; Castillo, P.E.; Davies, P. Age-dependent impairment of cognitive and synaptic function in the htau mouse model of tau pathology. *J. Neurosci.* **2009**, *29*, 10741–10749. [[CrossRef](#)]
90. Ward, S.M.; Himmelstein, D.S.; Lancia, J.K.; Binder, L.I. Tau oligomers and tau toxicity in neurodegenerative disease. *Biochem. Soc. Trans.* **2012**, *40*, 667–671. [[CrossRef](#)] [[PubMed](#)]
91. Hochdorffer, K.; Marz-Berberich, J.; Nagel-Steger, L.; Epple, M.; Meyer-Zaika, W.; Horn, A.H.; Sticht, H.; Sinha, S.; Bitan, G.; Schrader, T. Rational design of  $\beta$ -sheet ligands against A $\beta$ 42-induced toxicity. *J. Am. Chem. Soc.* **2011**, *133*, 4348–4358. [[CrossRef](#)] [[PubMed](#)]
92. Wagner, J.; Ryazanov, S.; Leonov, A.; Levin, J.; Shi, S.; Schmidt, F.; Prix, C.; Pan-Montojo, F.; Bertsch, U.; Mitteregger-Kretschmar, G.; et al. Anle138b: A novel oligomer modulator for disease-modifying therapy of neurodegenerative diseases such as prion and Parkinson's disease. *Acta Neuropathol.* **2013**, *125*, 795–813. [[CrossRef](#)]
93. Wagner, J.; Krauss, S.; Shi, S.; Ryazanov, S.; Steffen, J.; Miklitz, C.; Leonov, A.; Kleinknecht, A.; Gorick, B.; Weishaupt, J.H.; et al. Reducing tau aggregates with anle138b delays disease progression in a mouse model of tauopathies. *Acta Neuropathol.* **2015**, *130*, 619–631. [[CrossRef](#)] [[PubMed](#)]
94. Matthes, D.; Gapsys, V.; Griesinger, C.; de Groot, B.L. Resolving the atomistic modes of anle138b inhibitory action on peptide oligomer formation. *ACS Chem. Neurosci.* **2017**, *8*, 2791–2808. [[CrossRef](#)]
95. Belkacemi, A.; Doggui, S.; Dao, L.; Ramassamy, C. Challenges associated with curcumin therapy in Alzheimer disease. *Expert Rev. Mol. Med.* **2011**, *13*, e34. [[CrossRef](#)]
96. Mishra, S.; Patel, S.; Halpani, C.G. Recent updates in curcumin pyrazole and isoxazole derivatives: Synthesis and biological application. *Chem. Biodivers.* **2019**, *16*, e1800366. [[CrossRef](#)]
97. Chainoglou, E.; Hadjipavlou-Litina, D. Curcumin in health and diseases: Alzheimer's disease and curcumin analogues, derivatives, and hybrids. *Int. J. Mol. Sci.* **2020**, *21*, 1975. [[CrossRef](#)]
98. Narlawar, R.; Pickhardt, M.; Leuchtenberger, S.; Baumann, K.; Krause, S.; Dyrks, T.; Weggen, S.; Mandelkow, E.; Schmidt, B. Curcumin-derived pyrazoles and isoxazoles: Swiss army knives or blunt tools for Alzheimer's disease? *ChemMedChem* **2008**, *3*, 165–172. [[CrossRef](#)]
99. Liu, Y.; Dargusch, R.; Maher, P.; Schubert, D. A broadly neuroprotective derivative of curcumin. *J. Neurochem.* **2008**, *105*, 1336–1345. [[CrossRef](#)]
100. Valera, E.; Dargusch, R.; Maher, P.A.; Schubert, D. Modulation of 5-lipoxygenase in proteotoxicity and Alzheimer's disease. *J. Neurosci.* **2013**, *33*, 10512–10525. [[CrossRef](#)]
101. Kotani, R.; Urano, Y.; Sugimoto, H.; Noguchi, N. Decrease of amyloid- $\beta$  levels by curcumin derivative via modulation of amyloid- $\beta$  protein precursor trafficking. *J. Alzheimers Dis.* **2017**, *56*, 529–542. [[CrossRef](#)]
102. Okuda, M.; Hijikuro, I.; Fujita, Y.; Teruya, T.; Kawakami, H.; Takahashi, T.; Sugimoto, H. Design and synthesis of curcumin derivatives as tau and amyloid  $\beta$  dual aggregation inhibitors. *Bioorg. Med. Chem. Lett.* **2016**, *26*, 5024–5028. [[CrossRef](#)]
103. Okuda, M.; Fujita, Y.; Hijikuro, I.; Wada, M.; Uemura, T.; Kobayashi, Y.; Waku, T.; Tanaka, N.; Nishimoto, T.; Izumi, Y.; et al. PE859, a novel curcumin derivative, inhibits amyloid- $\beta$  and tau aggregation, and ameliorates cognitive dysfunction in senescence-accelerated mouse prone 8. *J. Alzheimers Dis.* **2017**, *59*, 313–328. [[CrossRef](#)] [[PubMed](#)]

104. Menniti, F.S.; Faraci, W.S.; Schmidt, C.J. Phosphodiesterases in the CNS: Targets for drug development. *Nat. Rev. Drug. Discov.* **2006**, *5*, 660–670. [[CrossRef](#)]
105. Bender, A.T.; Beavo, J.A. Cyclic nucleotide phosphodiesterases: Molecular regulation to clinical use. *Pharmacol. Rev.* **2006**, *58*, 488–520. [[CrossRef](#)]
106. Prickaerts, J.; Heckman, P.R.A.; Blokland, A. Investigational phosphodiesterase inhibitors in phase I and phase II clinical trials for Alzheimer's disease. *Expert. Opin. Investig. Drugs* **2017**, *26*, 1033–1048. [[CrossRef](#)]
107. Cuadrado-Tejedor, M.; Hervias, I.; Ricobaraza, A.; Puerta, E.; Perez-Roldan, J.M.; Garcia-Barroso, C.; Franco, R.; Aguirre, N.; Garcia-Osta, A. Sildenafil restores cognitive function without affecting  $\beta$ -amyloid burden in a mouse model of Alzheimer's disease. *Br. J. Pharmacol.* **2011**, *164*, 2029–2041. [[CrossRef](#)]
108. Heckman, P.R.; Wouters, C.; Prickaerts, J. Phosphodiesterase inhibitors as a target for cognition enhancement in aging and Alzheimer's disease: A translational overview. *Curr. Pharm. Des.* **2015**, *21*, 317–331. [[CrossRef](#)]
109. Li, P.; Zheng, H.; Zhao, J.; Zhang, L.; Yao, W.; Zhu, H.; Beard, J.D.; Ida, K.; Lane, W.; Snell, G.; et al. Discovery of potent and selective inhibitors of phosphodiesterase 1 for the treatment of cognitive impairment associated with neurodegenerative and neuropsychiatric diseases. *J. Med. Chem.* **2016**, *59*, 1149–1164. [[CrossRef](#)] [[PubMed](#)]
110. Lakics, V.; Karran, E.H.; Boess, F.G. Quantitative comparison of phosphodiesterase mRNA distribution in human brain and peripheral tissues. *Neuropharmacology* **2010**, *59*, 367–374. [[CrossRef](#)]
111. Shimizu-Albergine, M.; Rybalkin, S.D.; Rybalkina, I.G.; Feil, R.; Wolfsgruber, W.; Hofmann, F.; Beavo, J.A. Individual cerebellar Purkinje cells express different cGMP phosphodiesterases (PDEs): In vivo phosphorylation of cGMP-specific PDE (PDE5) as an indicator of cGMP-dependent protein kinase (PKG) activation. *J. Neurosci.* **2003**, *23*, 6452–6459. [[CrossRef](#)]
112. Puzzo, D.; Staniszewski, A.; Deng, S.X.; Privitera, L.; Leznik, E.; Liu, S.; Zhang, H.; Feng, Y.; Palmeri, A.; Landry, D.W.; et al. Phosphodiesterase 5 inhibition improves synaptic function, memory, and amyloid- $\beta$  load in an Alzheimer's disease mouse model. *J. Neurosci.* **2009**, *29*, 8075–8086. [[CrossRef](#)] [[PubMed](#)]
113. Zhang, J.; Guo, J.; Zhao, X.; Chen, Z.; Wang, G.; Liu, A.; Wang, Q.; Zhou, W.; Xu, Y.; Wang, C. Phosphodiesterase-5 inhibitor sildenafil prevents neuroinflammation, lowers beta-amyloid levels and improves cognitive performance in APP/PS1 transgenic mice. *Behav. Brain Res.* **2013**, *250*, 230–237. [[CrossRef](#)] [[PubMed](#)]
114. Schultheiss, D.; Muller, S.V.; Nager, W.; Stief, C.G.; Schlote, N.; Jonas, U.; Asvestis, C.; Johannes, S.; Munte, T.F. Central effects of sildenafil (Viagra) on auditory selective attention and verbal recognition memory in humans: A study with event-related brain potentials. *World J. Urol.* **2001**, *19*, 46–50. [[CrossRef](#)]
115. Fisher, D.A.; Smith, J.F.; Pillar, J.S.; St Denis, S.H.; Cheng, J.B. Isolation and characterization of PDE9A, a novel human cGMP-specific phosphodiesterase. *J. Biol. Chem.* **1998**, *273*, 15559–15564. [[CrossRef](#)]
116. Kleiman, R.J.; Chapin, D.S.; Christoffersen, C.; Freeman, J.; Fonseca, K.R.; Geoghegan, K.F.; Grimwood, S.; Guanowsky, V.; Hajos, M.; Harms, J.F.; et al. Phosphodiesterase 9A regulates central cGMP and modulates responses to cholinergic and monoaminergic perturbation in vivo. *J. Pharmacol. Exp. Ther.* **2012**, *341*, 396–409. [[CrossRef](#)]
117. Verhoest, P.R.; Fonseca, K.R.; Hou, X.; Proulx-Lafrance, C.; Corman, M.; Helal, C.J.; Claffey, M.M.; Tuttle, J.B.; Coffman, K.J.; Liu, S.; et al. Design and discovery of 6-[(3S,4S)-4-methyl-1-(pyrimidin-2-ylmethyl)pyrrolidin-3-yl]-1-(tetrahydro-2H-pyran-4-yl)-1,5-dihydro-4H-pyrazolo[3,4-d]pyrimidin-4-one (PF-04447943), a selective brain penetrant PDE9A inhibitor for the treatment of cognitive disorders. *J. Med. Chem.* **2012**, *55*, 9045–9054.
118. Schwam, E.M.; Nicholas, T.; Chew, R.; Billing, C.B.; Davidson, W.; Ambrose, D.; Altstiel, L.D. A multicenter, double-blind, placebo-controlled trial of the PDE9A inhibitor, PF-04447943, in Alzheimer's disease. *Curr. Alzheimer Res.* **2014**, *11*, 413–421. [[CrossRef](#)]
119. Moschetti, V.; Boland, K.; Feifel, U.; Hoch, A.; Zimdahl-Gelling, H.; Sand, M. First-in-human study assessing safety, tolerability and pharmacokinetics of BI 409306, a selective phosphodiesterase 9A inhibitor, in healthy males. *Br. J. Clin. Pharmacol.* **2016**, *82*, 1315–1324. [[CrossRef](#)]
120. Rosenbrock, H.; Giovannini, R.; Schanzle, G.; Koros, E.; Runge, F.; Fuchs, H.; Marti, A.; Reymann, K.G.; Schroder, U.H.; Fedele, E.; et al. The novel phosphodiesterase 9A inhibitor BI 409306 increases cyclic guanosine monophosphate levels in the brain, promotes synaptic plasticity, and enhances memory function in rodents. *J. Pharmacol. Exp. Ther.* **2019**, *371*, 633–641. [[CrossRef](#)]
121. Ghosh, A.S.; Wang, B.; Pozniak, C.D.; Chen, M.; Watts, R.J.; Lewcock, J.W. DLK induces developmental neuronal degeneration via selective regulation of proapoptotic JNK activity. *J. Cell. Biol.* **2011**, *194*, 751–764. [[CrossRef](#)]
122. Pozniak, C.D.; Sengupta Ghosh, A.; Gogineni, A.; Hanson, J.E.; Lee, S.H.; Larson, J.L.; Solanoy, H.; Bustos, D.; Li, H.; Ngu, H.; et al. Dual leucine zipper kinase is required for excitotoxicity-induced neuronal degeneration. *J. Exp. Med.* **2013**, *210*, 2553–2567. [[CrossRef](#)]
123. Le Pichon, C.E.; Meilandt, W.J.; Dominguez, S.; Solanoy, H.; Lin, H.; Ngu, H.; Gogineni, A.; Sengupta Ghosh, A.; Jiang, Z.; Lee, S.H.; et al. Loss of dual leucine zipper kinase signaling is protective in animal models of neurodegenerative disease. *Sci. Transl. Med.* **2017**, *9*, eaag0394. [[CrossRef](#)]
124. Patel, S.; Cohen, F.; Dean, B.J.; De La Torre, K.; Deshmukh, G.; Estrada, A.A.; Ghosh, A.S.; Gibbons, P.; Gustafson, A.; Huestis, M.P.; et al. Discovery of dual leucine zipper kinase (DLK, MAP3K12) inhibitors with activity in neurodegeneration models. *J. Med. Chem.* **2015**, *58*, 401–418. [[CrossRef](#)]
125. Patel, S.; Harris, S.F.; Gibbons, P.; Deshmukh, G.; Gustafson, A.; Kellar, T.; Lin, H.; Liu, X.; Liu, Y.; Liu, Y.; et al. Scaffold-hopping and structure-based discovery of potent, selective, and brain penetrant N-(1H-pyrazol-3-yl)pyridin-2-amine inhibitors of dual leucine zipper kinase (DLK, MAP3K12). *J. Med. Chem.* **2015**, *58*, 8182–8199. [[CrossRef](#)]

126. Patel, S.; Meilandt, W.J.; Erickson, R.I.; Chen, J.; Deshmukh, G.; Estrada, A.A.; Fuji, R.N.; Gibbons, P.; Gustafson, A.; Harris, S.F.; et al. Selective inhibitors of dual leucine zipper kinase (DLK, MAP3K12) with activity in a model of Alzheimer's disease. *J. Med. Chem.* **2017**, *60*, 8083–8102. [[CrossRef](#)]
127. Shih, J.C.; Chen, K.; Ridd, M.J. Monoamine oxidase: From genes to behavior. *Annu. Rev. Neurosci.* **1999**, *22*, 197–217. [[CrossRef](#)]
128. Sherif, F.; Gottfries, C.G.; Alafuzoff, I.; Oreland, L. Brain gamma-aminobutyrate aminotransferase (GABA-T) and monoamine oxidase (MAO) in patients with Alzheimer's disease. *J. Neural. Transm.* **1992**, *4*, 227–240. [[CrossRef](#)]
129. Kennedy, B.P.; Ziegler, M.G.; Alford, M.; Hansen, L.A.; Thal, L.J.; Masliah, E. Early and persistent alterations in prefrontal cortex MAO A and B in Alzheimer's disease. *J. Neural. Transm.* **2003**, *110*, 789–801. [[CrossRef](#)] [[PubMed](#)]
130. Saura, J.; Luque, J.M.; Cesura, A.M.; Prada, M.D.; Chan-Palay, V.; Huber, G.; Löffler, J.; Richards, J.G. Increased monoamine oxidase b activity in plaque-associated astrocytes of Alzheimer brains revealed by quantitative enzyme radioautography. *Neuroscience* **1994**, *62*, 15–30. [[CrossRef](#)]
131. Zhao, Y.; Zhao, B. Oxidative stress and the pathogenesis of alzheimer's disease. *Oxid. Med. Cell. Longev.* **2013**, *2013*, 316523. [[CrossRef](#)]
132. Sano, M.; Ernesto, C.; Thomas, R.G.; Klauber, M.R.; Schafer, K.; Grundman, M.; Woodbury, P.; Growdon, J.; Cotman, C.W.; Pfeiffer, E.; et al. A controlled trial of selegiline, alpha-tocopherol, or both as treatment for Alzheimer's disease. *N. Engl. J. Med.* **1997**, *336*, 1216–1222. [[CrossRef](#)]
133. Pisani, L.; Catto, M.; Leonetti, F.; Nicolotti, O.; Stefanachi, A.; Campagna, F.; Carotti, A. Targeting monoamine oxidases with multipotent ligands: An emerging strategy in the search of new drugs against neurodegenerative diseases. *Cur. Med. Chem.* **2011**, *18*, 4568–4587. [[CrossRef](#)] [[PubMed](#)]
134. Sterling, J.; Herzig, Y.; Goren, T.; Finkelstein, N.; Lerner, D.; Goldenberg, W.; Miskolczi, I.; Molnar, S.; Rantal, F.; Tamas, T.; et al. Novel Dual Inhibitors of AChE and MAO Derived from hydroxy aminoindan and phenethylamine as potential treatment for Alzheimer's disease. *J. Med. Chem.* **2002**, *45*, 5260–5279. [[CrossRef](#)]
135. Huang, L.; Lu, C.; Sun, Y.; Mao, F.; Luo, Z.; Su, T.; Jiang, H.; Shan, W.; Li, X. Multitarget-directed benzylideneindanone derivatives: Anti- $\beta$ -amyloid (A $\beta$ ) aggregation, antioxidant, metal chelation, and monoamine oxidase B (MAO-B) inhibition properties against Alzheimer's disease. *J. Med. Chem.* **2012**, *55*, 8483–8492. [[CrossRef](#)]
136. Tzvetkov, N.T.; Antonov, L. Subnanomolar indazole-5-carboxamide inhibitors of monoamine oxidase B (MAO-B) continued: Indications of iron binding, experimental evidence for optimised solubility and brain penetration. *J. Enzyme Inhib. Med. Chem.* **2017**, *32*, 960–967. [[CrossRef](#)]
137. Jayaraj, R.L.; Elangovan, N.; Dhanalakshmi, C.; Manivasagam, T.; Essa, M.M. CNB-001, a novel pyrazole derivative mitigates motor impairments associated with neurodegeneration via suppression of neuroinflammatory and apoptotic response in experimental Parkinson's disease mice. *Chem. Biol. Interact.* **2014**, *220*, 149–157. [[CrossRef](#)] [[PubMed](#)]
138. Ahsan, N.; Mishra, S.; Jain, M.K.; Surolia, A.; Gupta, S. Curcumin pyrazole and its derivative (N-(3-nitrophenyl)pyrazole) curcumin inhibit aggregation, disrupt fibrils and modulate toxicity of wild type and mutant  $\alpha$ -synuclein. *Sci. Rep.* **2015**, *5*, 9862. [[CrossRef](#)] [[PubMed](#)]
139. Deeg, A.A.; Reiner, A.M.; Schmidt, F.; Schueder, F.; Ryazanov, S.; Ruf, V.C.; Giller, K.; Becker, S.; Leonov, A.; Griesinger, C.; et al. Anle138b and related compounds are aggregation specific fluorescence markers and reveal high affinity binding to  $\alpha$ -synuclein aggregates. *Biochim. Biophys. Acta.* **2015**, *1850*, 1884–1890. [[CrossRef](#)]
140. Svenningsson, P.; Le Moine, C.; Fisone, G.; Fredholm, B.B. Distribution, biochemistry and function of striatal adenosine A<sub>2A</sub> receptors. *Prog. Neurobiol.* **1999**, *59*, 355–396. [[CrossRef](#)]
141. Schwarzschild, M.A.; Xu, K.; Oztas, E.; Petzer, J.P.; Castagnoli, K.; Castagnoli, N., Jr.; Chen, J.F. Neuroprotection by caffeine and more specific A<sub>2A</sub> receptor antagonists in animal models of Parkinson's disease. *Neurology* **2003**, *61*, S55–S61. [[CrossRef](#)]
142. Bara-Jimenez, W.; Sherzai, A.; Dimitrova, T.; Favit, A.; Bibbiani, F.; Gillespie, M.; Morris, M.J.; Mouradian, M.M.; Chase, T.N. Adenosine A<sub>2A</sub> receptor antagonist treatment of Parkinson's disease. *Neurology* **2003**, *61*, 293–296. [[CrossRef](#)]
143. Armentero, M.T.; Pinna, A.; Ferre, S.; Lanciego, J.L.; Muller, C.E.; Franco, R. Past, present and future of A<sub>2A</sub> adenosine receptor antagonists in the therapy of Parkinson's disease. *Pharmacol. Ther.* **2011**, *132*, 280–299. [[CrossRef](#)]
144. Yang, Z.; Li, X.; Ma, H.; Zheng, J.; Zhen, X.; Zhang, X. Replacement of amide with bioisosteres led to a new series of potent adenosine A<sub>2A</sub> receptor antagonists. *Bioorg. Med. Chem. Lett.* **2014**, *24*, 152–155. [[CrossRef](#)]
145. Zheng, J.; Yang, Z.; Li, X.; Li, L.; Ma, H.; Wang, M.; Zhang, H.; Zhen, X.; Zhang, X. Optimization of 6-heterocyclic-2-(1H-pyrazol-1-yl)-N-(pyridin-2-yl)pyrimidin-4-amine as potent adenosine A<sub>2A</sub> receptor antagonists for the treatment of Parkinson's disease. *ACS Chem. Neurosci.* **2014**, *5*, 674–682. [[CrossRef](#)]
146. Yang, Z.; Li, L.; Zheng, J.; Ma, H.; Tian, S.; Li, J.; Zhang, H.; Zhen, X.; Zhang, X. Identification of a new series of potent adenosine A<sub>2A</sub> receptor antagonists based on 4-amino-5-carbonitrile pyrimidine template for the treatment of Parkinson's disease. *ACS Chem. Neurosci.* **2016**, *7*, 1575–1584. [[CrossRef](#)]
147. Soderling, S.H.; Bayuga, S.J.; Beavo, J.A. Isolation and characterization of a dual-substrate phosphodiesterase gene family: PDE10A. *Proc. Natl. Acad. Sci. USA* **1999**, *96*, 7071–7076. [[CrossRef](#)] [[PubMed](#)]
148. Sancesario, G.; Morrone, L.A.; D'Angelo, V.; Castelli, V.; Ferrazzoli, D.; Sica, F.; Martorana, A.; Sorge, R.; Cavaliere, F.; Bernardi, G.; et al. Levodopa-induced dyskinesias are associated with transient down-regulation of cAMP and cGMP in the caudate-putamen of hemiparkinsonian rats: Reduced synthesis or increased catabolism? *Neurochem. Int.* **2014**, *79*, 44–56. [[CrossRef](#)]

149. Niccolini, F.; Foltynie, T.; Reis Marques, T.; Muhlert, N.; Tziortzi, A.C.; Searle, G.E.; Natesan, S.; Kapur, S.; Rabiner, E.A.; Gunn, R.N.; et al. Loss of phosphodiesterase 10A expression is associated with progression and severity in Parkinson's disease. *Brain* **2015**, *138*, 3003–3015. [[CrossRef](#)] [[PubMed](#)]
150. Movsesian, M.; Stehlik, J.; Vandeput, F.; Bristow, M.R. Phosphodiesterase inhibition in heart failure. *Heart Fail. Rev.* **2009**, *14*, 255–263. [[CrossRef](#)] [[PubMed](#)]
151. Heaslip, R.J.; Evans, D.Y. Emetic, central nervous system, and pulmonary activities of rolipram in the dog. *Eur. J. Pharmacol.* **1995**, *286*, 281–290. [[CrossRef](#)]
152. Verhoest, P.R.; Chapin, D.S.; Corman, M.; Fonseca, K.; Harms, J.F.; Hou, X.; Marr, E.S.; Menniti, F.S.; Nelson, F.; O'Connor, R.; et al. Discovery of a novel class of phosphodiesterase 10A inhibitors and identification of clinical candidate 2-[4-(1-methyl-4-pyridin-4-yl-1H-pyrazol-3-yl)-phenoxy-methyl]-quinoline (PF-2545920) for the treatment of schizophrenia. *J. Med. Chem.* **2009**, *52*, 5188–5196. [[CrossRef](#)] [[PubMed](#)]
153. Li, J.; Jin, H.; Zhou, H.; Rothfuss, J.; Tu, Z. Synthesis and in vitro biological evaluation of pyrazole group-containing analogues for PDE10A. *MedChemComm* **2013**, *4*, 443–449. [[CrossRef](#)] [[PubMed](#)]
154. Li, J.; Zhang, X.; Jin, H.; Fan, J.; Flores, H.; Perlmutter, J.S.; Tu, Z. Synthesis of fluorine-containing phosphodiesterase 10a (PDE10A) inhibitors and the in vivo evaluation of F-18 labeled PDE10A PET tracers in rodent and nonhuman primate. *J. Med. Chem.* **2015**, *58*, 8584–8600. [[CrossRef](#)] [[PubMed](#)]